DEGREE PROJECT IN TECHNOLOGY,
SECOND CYCLE, 30 CREDITS
STOCKHOLM, SWEDEN 2020

Modelling and Control of a Dual Sided Linear Induction Motor for a scaled Hyperloop pod

KTH Thesis Report

<Vivek Anand>

KTH ROYAL INSTITUTE OF TECHNOLOGY
SCHOOL OF ENGINEERING SCIENCES

Authors

Vivek Anand <vanand@kth.se>
Vehicle Engineering
KTH Royal Institute of Technology

Place for Project

Stockholm, Sweden
ITRL

Examiner

Mikael Nybacka
Teknikringen 8, 114 28 Stockholm
KTH Royal Institute of Technology

Supervisor

Luca Perretti
Teknikringen 33, 11428 Stockholm
KTH Royal Institute of Technology

Abstract

The electrification era has been marked up by an increase in volume of electric vehicles which are directly or indirectly powered by electricity. Railways, roadways and airways are being electrified as we speak at their own respective rate. In addition to that upcoming concepts for transport solution such as hyperloop also described as the fifth mode of transportation will be electrified. The current thesis work is based on developing the model and control of the propulsion system of a scaled Hyperloop pod designed by student team KTH Hyperloop representing KTH. The team competes in Hyperloop competition organized by Spacex and the goal is to achieve the highest possible speed in a given distance and track designed by SpaceX.

In order to achieve the goal of being the fastest, the scaled pod uses a Double Sided Linear Induction Motor (DSLIM) as mentioned in the subsequent chapter. The motor modelling is done on Simulink and is similar to a rotary induction motor (RIM). However the presence of end effect in DSLIM makes it different from RIM and has been discussed subsequently. The control strategy uses a synchronous frame PI control for the current control and sensor based speed control for controlling the speed of the pod.The speed control output is a reference current which is used as an input to the current controller which finally gives voltage as the control output. The corresponding bandwidth for the various loops have been calculated based on motor parameters as discussed in the method section.

The validation of the motor model and the corresponding controller has been discussed in the result section, where the accuracy of the controller for the designed modelled is discussed.

Keywords

Linear Induction Motor, Rotary Induction Motor, Control algorithm, bandwidth, Synchronous frame, Field weakening, Inductance, Resistance,PI controller, Magnetic flux, Mutual Inductance,Rise time, Error

Abstract

Elektrifieringstiden har präglats av en ökning i volym av elfordon som direkt eller indirekt drivs med el. Järnvägar, vägar och luftvägar elektrifieras just nu med deras respektive takt. Utöver det kommer kommande koncept för transportlösning som hyperloop som också beskrivs som det femte transportsättet att elektrifieras. Detta examensarbete bygger på att utveckla modellen och regleringen av framdrivningssystemet för en nedskalad Hyperloop-pod utvecklad av studentteamet KTH Hyperloop som representerar KTH. Teamet tävlar i Hyperloop-tävlingen organiserad av SpaceX och målet är att uppnå högsta möjliga hastighet på ett visst avstånd och spår framtaget av SpaceX.

För att uppnå målet om att vara snabbast använder den nedskalade podden en dubbelsidig elektrisk linjär induktionsmotor (DSLIM) som nämns i det följande kapitlet. Den elektriska motormodelleringen görs i Simulink och liknar en roterande induktionsmotor(RIM). Men närvaron av ’end effect’ i DSLIM gör den annorlunda än RIM och har diskuterats därefter. Styrstrategin använder en synkron ram-PI-styrning för strömstyrning och sensorbaserad hastighetsreglering för att styra hastigheten på podden. Varvtalsstyrningsutgången är en referensström som används som en ingång till den nuvarande styrenheten som slutligen ger spänning som slutling styrning. Motsvarande bandbredd för de olika slingorna har beräknats baserat på elektriska motorparametrar som diskuterats i metodavsnittet.Valideringen av elmotormodellen och motsvarande styrenhet har diskuterats i resultatsektionen, där noggrannheten hos styrenheten för den konstruerade modellerna diskuteras.

Nyckelord

Roterande induktionsmotor, styralgorithm, bandbredd, synkron ram, induktans, moststånd, PI-regulator, magnetiskt flöde, ömsesidig induktans, stingningstid, fel, Linjär induktionsmotor

Acknowledgements

This thesis experience has been one of the most challenging and eventful experience during my master studies at KTH. The decision to work on a topic which stands outside the domain of my then current knowledge was on one hand captivating and on the other hand a big challenge to surmount. But now I am pleased to have taken this challenge and am grateful to everyone who has supported me during this thesis work.

I would like to begin by thanking my supervisor Dr Luca Peretti, who has encouraged me to take this thesis topic and in a way has given me the confidence to undertake this challenge. My thank also goes to my Examiner Dr Mikael Nybacka who has been a constant guide throughout my Master studies and have supported me during my thesis as well. Moving on I would like to thank the entire team of KTH Hyperloop 2018/19 in general and the 'Propulsion team' in particular, for their knowledge sharing which made me capable enough to peek and explore this unknown territory of controlling Electrical Machines moreover I would like to thank supervisors from our KTH Hypelroop team Claes Eriksson and Rocco Giossi for their feedback.

In addition to that I am grateful to the entire ITRL team and staffs for allowing me to start the Hyperloop project at the beginning of my Masters and in a way giving me the opportunity to conclude my Masters through this thesis. ITRL became and KTH Hyperloop became my second home and family in Sweden. I am also grateful to the department of Vehicle Engineering, Professor Lars Drugge and Professor Jenny Jerrelind for their constant help and support during my studies.

The list is long but I would like to take some time out to especially thank few more people who have helped me during this thesis. Thank you Bhanu Singh, Aswini Manoharan and Jay Prakash for all the fruitful discussions, suggestions and help during the thesis work. Furthermore I am thankful to all my friends in Sweden and in India who were there to encourage me during the stressful time.

And last but not the least I would like to thank my family in India. I am ever grateful to

my parents for giving me the opportunity to pursue my dreams and my elder brother Abhishek for navigating me to it, I will be ever indebted to them.

Acronyms

LIM	Linear Induction Motor
RIM	Rotary Induction Motor
DSLIM	Double Sided Linear Induction Motor
V/f	Voltage/frequency
FOC	Field Oriented Control
VFD	Variable Frequency Drive
DFO	Direct Field Orientation
IFO	Indirect Field Orientation
DTC	Direct Torque Control
MMF	Magneto Motive Force

Contents

Chapter 1

Introduction

Linear Induction Motor (LIM) unlike their counterpart Rotary Induction Motor (RIM) which are frequently used in majority of applications are slowly catching up. The simplicity in its design, high value of initially produced thrust force and low noise has made its application suitable in different fields such as transportation, actuation, elevators, robotics and automation. DSLIM which is a special arrangement involving LIM follows the same electromagnetic behavior as a single sided linear induction motor.

1.1 Brief Introduction to DSLIM

The DSLIM is a type of linear induction motor arrangement which produces an equal and opposite linear force on both the primary and secondary. Thereafter depending on which of them are set to have the linear degree of freedom are subjected to Linear motion. Therefore we can have two different arrangements for DSLIM, one where primary is fixed and secondary is moving and vice versa. The operating principle remains similar to a rotary induction machines with a slight difference due to end effect in DSLIM.

1.2 Background

The thesis is done in collaboration with KTH Royal Institute Of Technology and KTH Hypelroop at Integrated Transport Research Lab (ITRL). The subject is developing

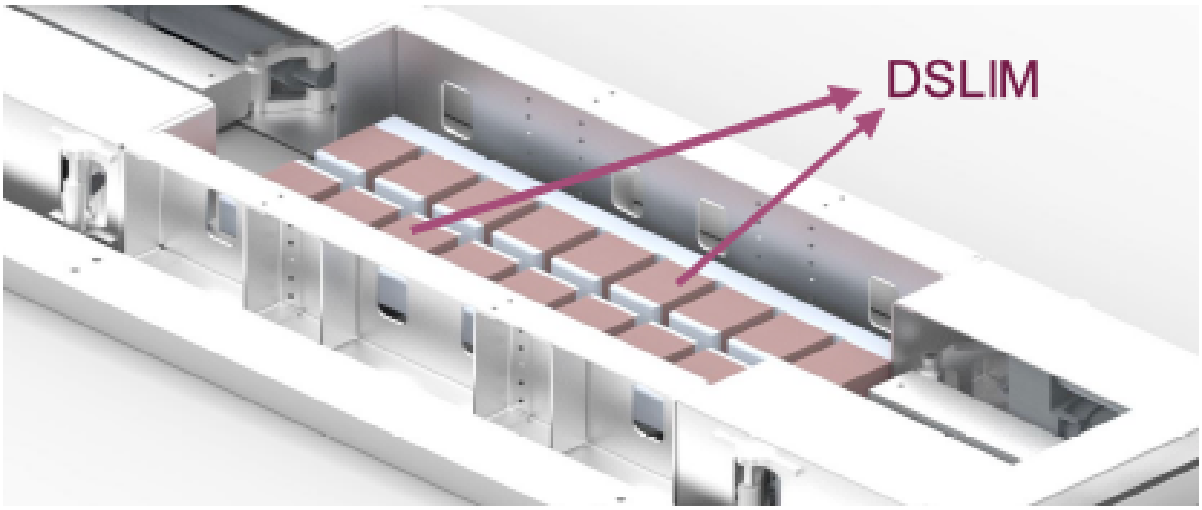

Figure 1.2.1: Placement of DSLIM around the I beam

a model of a DSLIM and a control algorithm for the same based on MATLAB and Simulink. The scaled hyperloop pod designed by KTH Hyperloop has an indigenously developed DSLIM developed for the SpaceX Hyperloop Competition. The design and arrangement of the DSLIM in the pod is restricted by track constraints provided by SpaceX and the mechanical design constraint of the pod. The DSLIM consists of eight poles, and is basically a 3-phase motor. The motor winding is made of copper and has a single layer, with a ferromagnetic core on both sides of the I beam [1], as depicted in Figure 1.2.1

This arrangement gives the possibility of developing maximum flux linkage without requiring any back iron (ferromagnetic) plate. The generated thrust form DSLIM used for propelling the pod is mainly dependent on three factors, which are listed below:

- Air gar gap between the I beam and the stator: The generated magnetic flux is greatly affected by this gap. The selection of this gap is dependent on allowed tolerance for ensuring lateral stability of the pod and the curvature along the line of displacement.
- Maximum on board supply voltage: The design of the DSLIM is centered around the maximum possible supplied voltage. Where the supplied Voltage is limited due to on board safety, addition of mass to the pod and the maximum current that can be drawn by the motor winding.

[1]The I beam is an aluminium rail passing through the center

- Length of the pod/LIM: The length of the LIM is directly associated with the maximum velocity as shown in the given relation.

$$V_{sync} = 2f\tau \tag{1.1}$$

  Where, V_{sync}, f and τ are Synchronous velocity, applied frequency, and pole pitch respectively.

Given these main constraints the maximum thrust produced by a DSLIM of a given length is obtained for different stator frequency. Once the variation of thrust force with respect to Stator frequency is known a controller is designed in order to control the dynamics of DSLIM model for generating the correct output voltage signal for reaching the required thrust force for a generated trajectory. This is also the main theme of this thesis, problems related to design optimization of Linear Motor, improving the thermal and electrical efficiency are not a part of this study.

1.3 Problem

Given the DSLIM of a length of 1.4 m capable of generating a thrust force of 2400 N for different operating frequencies supplied by a DC voltage source of 500V, we would want to design:

- A DSLIM Model in SIMULINK environment
- A Current and Speed controller using vector control method for the designed model
- A Field Weakening controller
- Using a required Load trajectory at various speed as feedback to the DSLIM Model

The problem narrows down to generating a control algorithm or method for a constrained model where the goal is to achieve the highest speed in a given distance of 1.2km in a straight line trajectory.

Present the problems found in the area. Preferable use and end this section with a question as a problem statement.

1.4 Purpose

The main purpose of this thesis is to illustrate and discuss the method for developing a motor model and its controller such that it can pave the way for further developing this work for an actual implementation on a scaled Hyperloop pod.

The thesis report is also meant to lay down and highlight the scope for future work weighing down the practical implementation for the competition and more research oriented approach.

1.5 Goal

The expected outcomes or goals for this thesis are listed below:

- A motor model designed in simulink with an expected load for the given trajectory.
- A vector control method modeled in Simulink along with a field weakening controller.
- An expected behavior of the controller where the target speed is achieved with less overshoot, and low rise time.
- Measuring the motor parameter and tuning the controller accordingly for the actual motor to be used in the Hyperloop system.

1.6 Benefits, ethics and sustainability

The Hyperloop concept was introduced back in 2013 by Elon Musk in his famous white paper[10]. The concept presents the possibility of travelling at a speed of 1200 Km/h in a levitating pod in a near vacuum tube. In order to give this idea a concretes shape SpaceX organises Hyperloop Pod competition where Student teams all across the globe try to build the fastest pod as they race their Hyperloop Pods in 1.2km long vacuum tube with a track. Last year the speed record of 463Km/h was set by one of the student teams.
This thesis aims at exploring the concept of Hyperloop as well as targets one of the most crucial system of this technology namely the propulsion. Not only this mode of transportation will reduce the travel time between two cities but will also allow people

to experience a sustainable expansion in their choice of living and livelihood. One example to show the impact of this technology is the calculation of travel time between Stockholm to Gothenburg (the two major cities of sweden), which will reduce to a mere 20 minutes travel (given no intermediate stops).
Since the system is imagined to be an all electric system it will greatly reduce the carbon footprints when compared to its close competitors in Aviation industry.In addition to that being an engineer its of utmost importance and really ethical that new ideas and technologies which have the capability to bring a revolution should be explored.

1.7 Delimitations

The main delimitation to this project is getting the correct model parameters from stationary, dynamic or simulation based testing of the LIM. Since identifying the parameters will further broaden the scope of this thesis, they have not been considered as the major objective of this thesis. However, their effect will be huge in determining the usefulness of the controller and its future practical implementation.

1.8 Outline

Having introduced the main objective and goal of the thesis, this section will give an overview of the subsequent chapters covering the breakdown of the thesis and brief description of the topics covered.

Chapter 2 Gives the the literature background behind the equivalent circuit for a LIM and how to model a DSLIM. Introduction to different control strategies used for controlling a LIM and DSLIM.

Chapter 3 Presents the three most suitable methods for controlling the DSLIM, their pros and cons and which method should be selected for this study.

Chapter 4 Describes in detail the modelling of the DSLIM model in Simulink.Also the detailed description of the method for designing the controller.

Chapter 5 Gives the obtained results and discusses the inter-dependency the

controller parameters and the motor parameters for getting a stable response.

Chapter 6 Describes and evaluate the results of the degree project, its success and drawbacks. Suggests the scope for improvement and future work.

Chapter 2

Literature review

2.1 General review

This chapter delves into the literature background of the thesis work.(also add type of LIM)

The background for any LIM model application boils down to the derived equivalent circuit of the motor. The derivation of Linear Induction motor equivalent circuit has been done in 1983 [3]. The rotary induction motor model was altered to include the end effect and the output thrust was satisfactorily predicted based on a test set up. It is also suggested that the equivalent circuit of a LIM and DSLIM will inherently be the same. In an another contemporary study where the speed control of a LIM is the main focus, derivation of the motor model is of particular interest [1]. Given the objective of this study is somewhat related to the current thesis work the equivalent circuit equations used in this study have been primarily used to model the motor model in the thesis work.

In the study undertaken in [9] the comparison between the control method as well as the modulation technique used for a LIM has been done. The study also demonstrates the modelling of the end effect present in LIM as an external load function proportional to velocity. The modulation technique is not in the scope of current thesis work, however the comparison between two different control strategies namely the PI and SMC is of interest. The variation in thrust force produced by a DSLIM due to the end effect has been the area of focus in [14].A mathematical model is derived to account for the dynamic end effect. In addition to that, a new field orientation is introduced to account for the flux change when secondary enters or leaves the primary region.

The DSLIM speed control has also been studied in [2] where the DSLIM is modelled, simulated and its parameters are determined. Constant Voltage/frequency (V/f) speed controller has been used in this study and the obtained results are compared with a test bench result. Even though V/f speed controller seems a simple and reliable way to control the speed, in this study we have not used V/f controller in order to have a robust speed controller in the outer loop. Nevertheless the approach is worth mentioning and could be investigated further.
In addition to that course book titled as 'Control of Voltage Source converter and variable speed drives' [7] provides an understanding of DC and AC motors from a basic level, also discussing in details the various control method and effect of motor parameters on designing the controller. The method for designing the controller as well as its subsequent analysis has been done in accordance with the sections discussed in this textbook. Moreover for developing an understanding of various control scheme used in Induction motor control other articles and textbook has also been referred. Electric Motor and Drives [4] , chapter 8 breaks down the fundamentals of Field oriented control and has been used to develop a robust understanding of the topic. The understanding of modern control methods available for Induction motor is presented in chapter 10 of Electric Motor Products [21] and has been used in selecting the control strategy for the current work.

2.2 Dominant Literature

This section discusses briefly some of the dominant literature in the field of the thesis problem. In one of the earliest work [20] which advocates the use of LIM as a propulsion system for a contact-less transportation the study of motor performance, end effect compensation as well as numerical derivation of the electromagnetic field in the air gap has been done. Another notable work as mentioned in the previous section in modelling LIM is done in [3] where the equivalent circuit of LIM is derived using the principle of RIM by accounting the end effect to it. In order to develop the fundamental understanding of electric machines in general and induction machines in particular the book 'Analysis of electrical machinery and drive systems' [6] has been dominantly referred. Furthermore, after identifying the goal and scope of the thesis the course book 'Control of voltage source converters and variable speed drives' [7] has been referred frequently. The modelling and control of the LIM with end

effect compensation using Vector control strategy and field oriented control has been discussed in [5] and [15] respectively. The methods described for designing the controller with end effect compensation could not be utilized due to limited time span of the thesis, however they act as a reference for future work. In addition to that in order to understand the scope of hyperloop pod competition organised by SpaceX and the various sub systems involved in the scaled hyperloop pod , the final design report of MIT Hyperloop and KTH Hyperloop have been referred [16, 17].

Chapter 3

Control method selection

There are various strategies for controlling a system, hence the selection of the most suitable control method is really important. The method for selecting the control strategy depends on the plant or system to be controlled and also the main objective or performance outcome expected from the plant.

3.1 Available meethods

The plant or the process that we would like to control here is a three phase electrical machine, with an objective that it must be able to correctly control the desired load force in order to achieve within the given trajectory a sufficiently high speed. Thus the problem we are trying to solve here is a Variable Frequency Drive (VFD) control problem. It should also be noted down that the scope of the thesis is limited by the timeline as well as the availability of the data and changes in the track length, hence in the design of the controller it is restricted to a continuous system and no discretization has been used. Therefore discussion regarding modulation technique has not been undertaken in this study.

The simplest or more traditional approach for controlling an induction machine or a VFD is to use a volt/hertz speed control method. This is an open loop control method where there is no prerequisite to know the speed and current value. Here a speed reference is used to vary the Primary voltage linearly with respect to the primary frequency. It should be noted that its a scalar control method. The relation is as given

below as

$$\omega_1 = \omega_{\text{ref}} + \widehat{\omega}_2$$
$$|\mathbf{v}_s| = \begin{cases} \frac{|\omega_1|}{\omega_{\text{base}}} V_{\text{base}}, & |\omega_1| \leq \omega_{\text{base}} \\ V_{\text{base}}, & |\omega_1| > \omega_{\text{base}} \end{cases} \tag{3.1}$$

$\widehat{\omega}2$ being the estimate of the slip frequency, ω_1 is stator (primary) voltage frequency, $|v_s|$ is the magnitude of stator voltage and V_{base} is the base Voltage. In [2] the V/f controller has been used where the nominal flux value is maintained by keeping the ratio of primary voltage and frequency as fixed. The LIM speed is thus controlled by changing the excitation frequency as well changing the driving primary voltage at the same time. In addition to that the error on the slider speed goes through an anti windup PI controller in order to provide a feedback control.
In general, the V/f controller has some drawbacks, it lacks the closed loop current control in primary which can lead to transient behaviors in flux and over current. Since these slow transients can lead to large to large torque oscillations it might be challenging to get a precise torque or speed control. The accuracy of the speed control is crucial for the problem described in this thesis therefore another control method which is widely used called Vector Control is considered. Moreover in [1], [9] and [14] Indirect Field Oriented Control (FOC) which is a type of vector control strategy has been used for controlling the SLIM and DSLIM respectively. The Vector control strategy in general and Indirect FOC in particular have been described in the next section.

3.2 Vector control/ field oriented control

It is expected in many applications including the one for this thesis problem that the electromagnetic torque should be controlled instantaneously to follow the reference or desired torque request. Given such a system it becomes much easier to have the speed control since the electrical dynamics becomes irrelevant to the mechanical dynamics. For achieving that kind of performance in induction machines we can rely on using a class of control algorithms referred to as field oriented control. Based on the orientation of flux there are three types of field oriented control namely rotor flux oriented, stator flux oriented and air gap flux oriented control. However here we will discuss the rotor (in our case secondary) flux oriented control in induction machines with two types of implementation namely direct and indirect.

In vector control, the ac motors are controlled using similar algorithms as in DC motors. This is made possible by using a rotating frame 'dq' which is made to synchronously rotate with motor's flux. Thereafter a current control algorithm is used in this frame.

Since it is difficult to measure the flux of an IM, a flux estimator is used for generating an estimate. If the secondary circuit model of an IM is used we get the 'Current model' flux estimator whereas if primary circuit model of an IM is used we get the 'Voltage model' flux estimator. Now depending whether the above mentioned flux estimators are implemented in $alpha\ beta$ or *dq* frame, we get the resulting vector control systems called Direct field orientation and indirect field orientation[7]. These two different approaches however allows the control of induction motor by using the same principle of decoupling the torque and flux [12]. In the subsequent sections we will discuss briefly about speed-sensored direct and indirect field orientation control system using 'Current Model'.

3.2.1 Direct field orientation

In order to estimate the flux of the IM, we use the secondary (rotor)[1]circuit equation of IM to obtain the following flux estimator:

$$\frac{d\widehat{\boldsymbol{\psi}}_R^s}{dt} = \widehat{R}_R \mathbf{i}_s^s - \left(\frac{\widehat{R}_R}{\widehat{L}_M} - j\omega_r \right) \widehat{\boldsymbol{\psi}}_R^s \tag{3.2}$$

Where $\widehat{\boldsymbol{\psi}}_R^s$ and $\mathbf{i}_s^s$ represents [2] rotor flux and stator current [3]in the stationary $\alpha\beta$ frame, $\widehat{R}_R$ represents the estimated rotor resistance, $\widehat{L}_M$ represents magnetizing inductance and ω_r represents the angular speed of the rotor.

The above equation represents the 'Current model' for flux estimation in $\alpha\beta$ frame, and hence the corresponding vector control system is called Direct Field Orientation (DFO).

DFO was preferred over Indirect Field Orientation (IFO) for analog implementation, however with the development of powerful and faster microprocessors which paved the way for implementing digital control IFO has overtaken DFO.

[1]We have developed the controller by using equations for RIM instead of LIM as discussed in subsequent chapters

[2]Here the subscript 'R' or 'r' represents rotor (secondary) parameters, whereas subscript 'S' or 's' represents stator (Primary) parameters.

[3]The superscript 's' represents the stationary $\alpha\beta$ frame.

3.2.2 Indirect field orientation

If we assume that in 3.2 the $\widehat{\psi}_R$ is real i.e, perfect field orientation then the above equation changes to following:

$$\frac{d\widehat{\boldsymbol{\psi}}_R^s}{dt} = \widehat{R}_R \mathbf{i}_s^s - \left(\frac{\widehat{R}_R}{\widehat{L}_M} + j\omega_2 \right) \widehat{\boldsymbol{\psi}}_R^s \tag{3.3}$$

If we separate the real and imaginary parts, we get [4]

$$\frac{d\widehat{\psi}_R}{dt} = \widehat{R}_R i_d - \frac{\widehat{R}_R}{\widehat{L}_M} \widehat{\psi}_R \tag{3.4}$$

$$\omega_2 = \omega_1 - \omega_r = \frac{\widehat{R}_R i_q}{\widehat{\psi}_R} \tag{3.5}$$

Equation 3.5 gives the slip relation. This relation is used to compute the angular frequency as shown below:

$$\omega_1 = \omega_r + \frac{\widehat{R}_R i_q^{\text{ref}}}{\widehat{\psi}_R}, \qquad \dot{\theta}_1 = \omega_1 \tag{3.6}$$

it should be noted that we use i_q^{ref} and i_d^{ref} in 3.6 and 3.7 respectively. This is done in order to remove the noise.

$$\frac{d\widehat{\psi}_R}{dt} = \widehat{R}_R i_d^{\text{ref}} - \frac{\widehat{R}_R}{\widehat{L}_M} \widehat{\psi}_R \tag{3.7}$$

The schematic of IFO control is shown below in 3.2.1 [7]:

In IFO, at steady state it is noted that all quantities except (beside θ_1) are constant, whereas we have ω_1 as a variable used in the control scheme. Therefore IFO is preferred over DFO while using the “Current Model” [7](page 183).

3.2.3 Direct torque control:

Another vector control strategy is Direct Torque Control (DTC) where we use stator flux as the reference frame instead of using rotor flux as shown previously in FOC. As

[4]The subscript ’d’ and ’q’ represents the parameter value in d and q axis respectively.

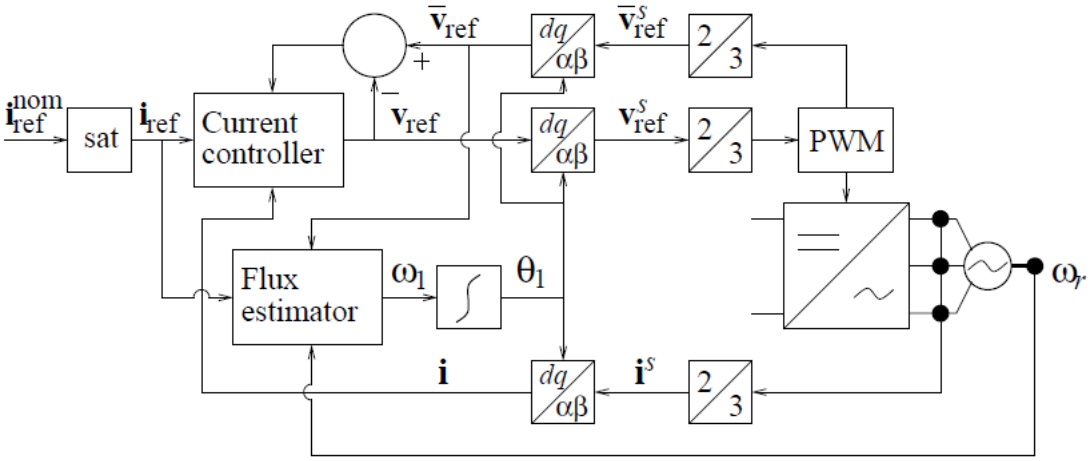

Figure 3.2.1: Control Scheme for IFO Vector control in Induction Motor

the name suggests DTC involves a direct control scheme for torque and flux, instead of controlling the stator current as done in FOC.

The control strategy looks for errors in torque and flux vector. Hysteresis control is then used to accordingly modify the primary (stator) voltage based on those errors. The control schematic is depicted as below [19]:

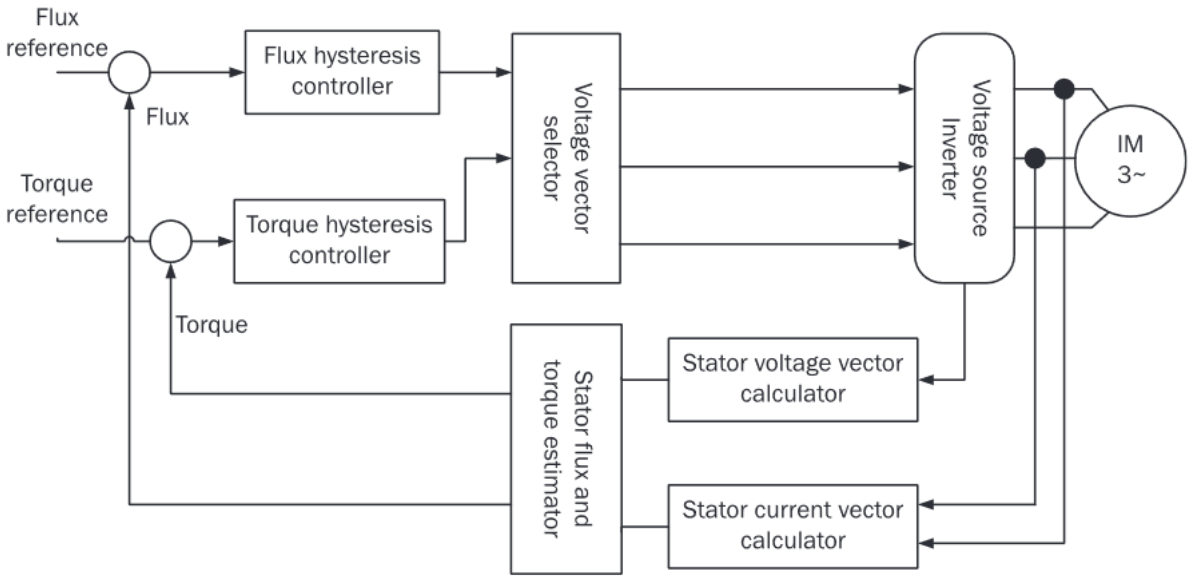

Figure 3.2.2: Control scheme for DTC control in induction motor

Thus we have covered some of the main control strategies frequently used for solving a variable frequency induction motor control problem. Based on the goal of the thesis problem, IFO speed sensored control stands out as a robust and tailored made solution.

Therefore, IFO Vector control scheme is used in the modelling section. It should however be noted that given the ease of implementation, the combination of field oriented control and v/f control could also serve as an ideal solution. In that control scheme we could have the possibility of having a closed current loop in dq frame which is missing in a traditional v/f controller. Whereas, the frequency controller can be used in the outer loop to determine the angular speed of dq frame based on the maximum torque(thrust in case of LIM) produced at a given frequency.

Chapter 4

Modelling

This chapter describes the majority of the actual thesis work which has been done and focuses on two most important modelling aspect of the thesis:

- Modelling the LIM
- Modelling the controller

4.1 Modelling of LIM

Before we proceed further It is important to understand the difference between LIM and RIM. As mentioned previously the existence of end effect makes the equivalent circuit of LIM different from its counterpart RIM. On the one hand, in RIM we have pole by pole symmetry whereas in LIM the electromagnetic behavior/response differs at the entry and exit point of the primary-secondary relative motion. How does the flux and thrust (torque in RIM) force differ in LIM with respect to RIM?
This is discussed in the next subsection.

4.1.1 End effect

LIM has been described in many literatures [1, 3] as RIM ”cut open and rolled flat”. In general there are many similarities between a RIM and LIM. And it is in a way correct to say that equivalent circuit model of a LIM and RIM should be same as long as the primary and secondary in a LIM do not have any relative motion.What happens when there is a relative motion?

To answer that question, we try to visualize the situation of a relative motion between primary and secondary. In this visualization we try to fix the secondary while the primary is moving. We notice that as the primary moves forward, the secondary is replaced by a new material at every instant. This happens at both front and rear of primary's corresponding secondary's section. The new secondary material coming under the influence of the primary's electromagnetic effect only allows a gradual change in the flux density in the air gap, while resisting a sudden change. Therefore it becomes utmost important to quantify this effect known as 'End effect' to get a robust equivalent circuit model of LIM.

Figure 4.4.1 [1] shows how the relative motion between the primary and secondary results in generation of eddy current at the entry and exit section of secondary [1, 5, 8, 15].

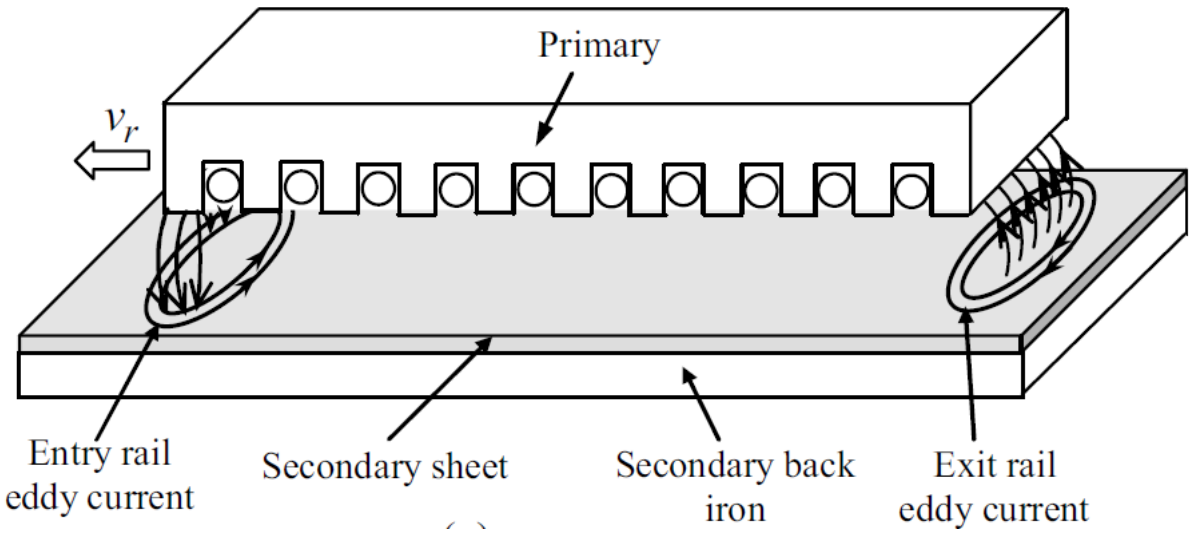

Figure 4.1.1: Generation of Eddy current in the LIM.

Note in the current study we have DSLIM and the primary is mirrored to the other side along secondary. The motor model for both SLIM and DSLIM have been assumed to have the same equivalent circuit. The differences however are accounted in terms of the motor parameter.

The eddy currents directly affect the corresponding Magneto Motive Force (MMF) of the primary, especially at the entry where the air gap flux is nearly reduced to zero. The eddy current density profile is shown in Figure 4.1.2 [1, 5, 8, 15]. In addition to that the corresponding air gap flux profile alongside the motor length is shown in Figure 4.1.3.

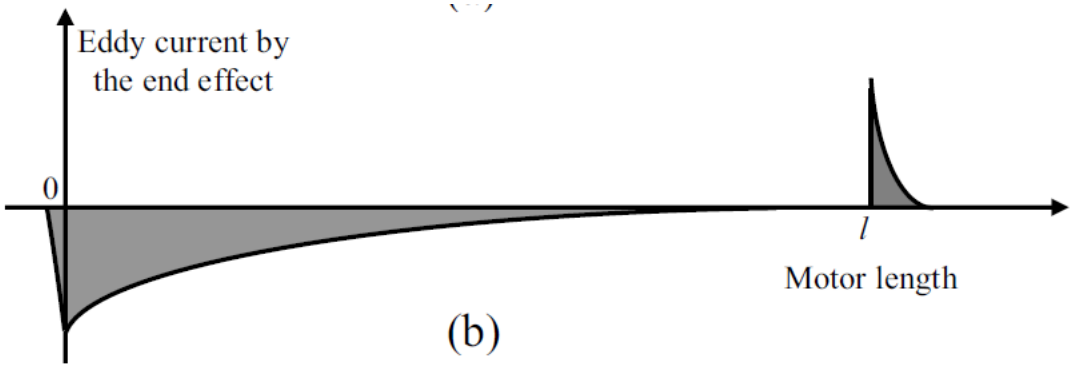

Figure 4.1.2: Eddy current generation due to end effect.

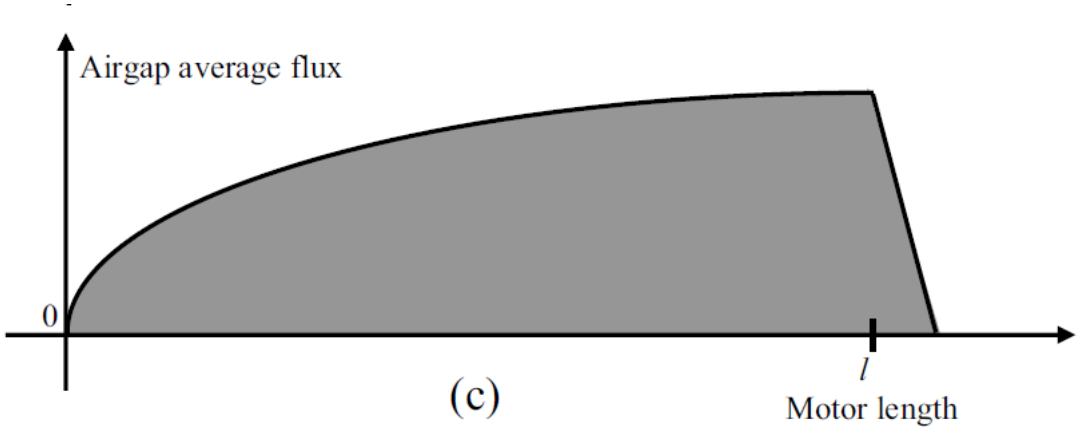

Figure 4.1.3: Air gap flux alongside motor length.

It can be seen that the air flux tends to zero at the entry point of new material as mentioned previously.

In addition to the air gap flux behavior, it is also seen that there is a thrust attenuation due to the relative motion between primary and secondary. This attenuation is a function of the relative velocity between the primary and the secondary and is proportional to it. Thus for a higher relative velocity the thrust attenuation is higher and vice versa [1, 5, 8, 13, 15]. Moreover the 'end effect' behavior varies depending whether material is at the point of entry or exit. This is attributed to the difference in the time constant at the current induced at entry and exit. Larger time constant leads to a slower decay at the entry and vice versa [1].

The end effect has been parameterized in terms of parameter Q as used by Duncan. The parameter Q relates the dependency of end effect on the length of primary as well as to the relative velocity of primary with respect to secondary [5, 8] as shown in Equation 4.1.

In an another representation [14] the end effect has been accounted for splitting

the equivalent circuit into valid and invalid region. This distinction is based on the relative position of primary with respect to secondary. The final model is obtained by summing up the mathematical model of the two regions. A coupling factor is introduced to account for the transformation relation between the two regions and the motor parameters. This representation is shown in Figure 4.1.4 [14].

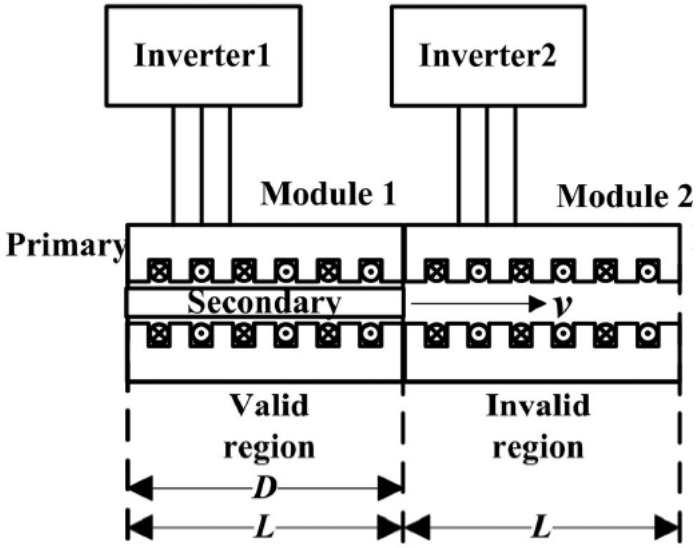

Figure 4.1.4: Accounting end effect by splitting the model in Valid/Invalid regions

Even though this approach seems intuitive, it is not used to model the equivalent circuit of the LIM in this thesis. This is primarily because the study uses relative motion between primary and secondary where the secondary is moving while primary is fixed and is multi inverted fed. Whereas in the thesis problem we have a single inverted fed LIM with a fixed secondary and moving primary as shown below.

4.1.2 Governing equation and Simulink model

The modelling of DSLIM uses the same set of governing equations as mentioned in [1] since the goal of this thesis work is to examine the scenario where primary moves with respect to secondary and not vice versa.

$$Q = \frac{l \cdot R_r}{L_r \cdot v_r} \tag{4.1}$$

$$L'_m = L_m(Q) = L_m(1 - f(Q)) \tag{4.2}$$

L_m is the zero speed magnetising inductance and $f(Q) = \left(1 - e^{-Q}\right)/Q$

The secondary and primary inductances are represented as [5, 8]:

$$L'_r = L_r(Q) = L_r - L_m f(Q) \tag{4.3}$$

$$L'_s = L_s(Q) = L_s - L_m f(Q) \tag{4.4}$$

Whereas the secondary time constant is represented as

$$\tau'_r = L'_r/R_r = L_r/R_r - L_m \cdot f(Q)/R_r \tag{4.5}$$

The voltage equation in dq [1]frame for primary and secondary is represented as follow [1, 5, 18]:

$$v_{ds} = R_s i_{ds} + R_r f(Q) \cdot (i_{ds} + i_{dr}) + p\phi_{ds} - \omega_e \phi_{qs} \tag{4.6}$$

$$v_{qs} = R_s i_{ds} + p\phi_{qs} + \omega_e \phi_{ds} \tag{4.7}$$

$$v_{dr} = R_r i_{dr} + R_r f(Q) \cdot (i_{ds} + i_{dr}) + p\phi_{dr} - (\omega_e - \omega_r)\, \phi_{qr} = 0 \tag{4.8}$$

$$v_{qr} = R_r i_{qr} + p\phi_{qr} + (\omega_e - \omega_r)\, \phi_{dr} = 0 \tag{4.9}$$

The linkage fluxes in the dq frame for primary and secondary are represented as follow:

$$\phi_{ds} = L_{ls} i_{ds} + L_m(1 - f(Q))\, (i_{ds} + i_{dr}) \tag{4.10}$$

$$\phi_{qs} = L_{ls} i_{qs} + L_m\, (i_{qs} + i_{qr}) \tag{4.11}$$

[1]The equations are written for RIM, where subscript r stands for rotor and in turn represents secondary, whereas subscript s denotes stator and in term represents primary

$$\phi_{dr} = L_{lr} i_{dr} + L_m(1 - f(Q))\,(i_{ds} + i_{dr}) \tag{4.12}$$

$$\phi_{qr} = L_{lr} i_{qr} + L_m\,(i_{ds} + i_{dr}) \tag{4.13}$$

$$F_e = \frac{3}{2} P \frac{\pi}{h} \frac{L_m(1 - f(Q))}{L_r - L_m f(Q)} \left(\phi^e_{dr} i^e_{qs} - \phi^e_{qr} i^e_{ds}\right) = M \cdot \dot{v}_r + D \cdot v_r + F_L \tag{4.14}$$

Here i_{ds}, i_{qs} are direct and quadrature secondary currents, k_p, k_i are proportional and integral actions of PI controller, L_s, L_r, L_m are primary, secondary and magnetizing inductances, L_{lr}, L_{ls} are primary and secondary leakage inductances, P is number of pairs of poles, R_s, R_r are primary and secondary resistances, D is viscous friction and iron-loss coefficient, M is the total mass of the moving element, v_{ds}, v_{qs} are direct and quadrature primary voltages, ϕ_{dr}, ϕ_{qr} are direct and quadrature secondary fluxes, τ_r is secondary time constant (L_r/R_r), v_e is synchronous velocity, v_r is linear velocity, v_{sl} is Slip velocity, Q is dimensionless factor, l is the primary length, h is pole pitch, F_e is thrust force, K_f is constant force and F_L is load force.

The above equations are modeled as shown below in Figures 4.1.5, 4.1.6 and 4.1.7 using Simulink to obtain the equivalent circuit model of the LIM. They respectively represent the flux equation, the voltage equation and equations related to calculation of Magnetizing inductance, torque production and effect variable.

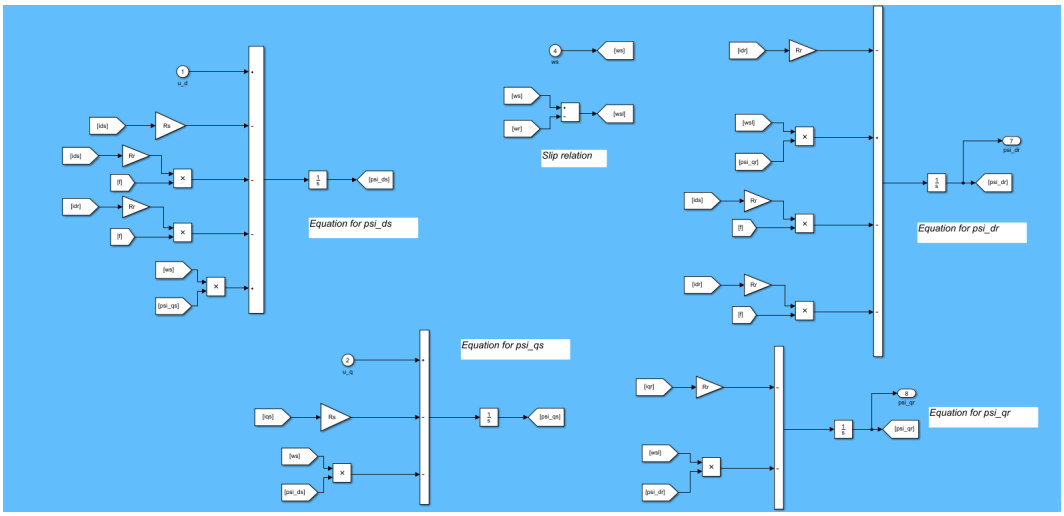

Figure 4.1.5: Flux equation in dq frame for primary and secondary.

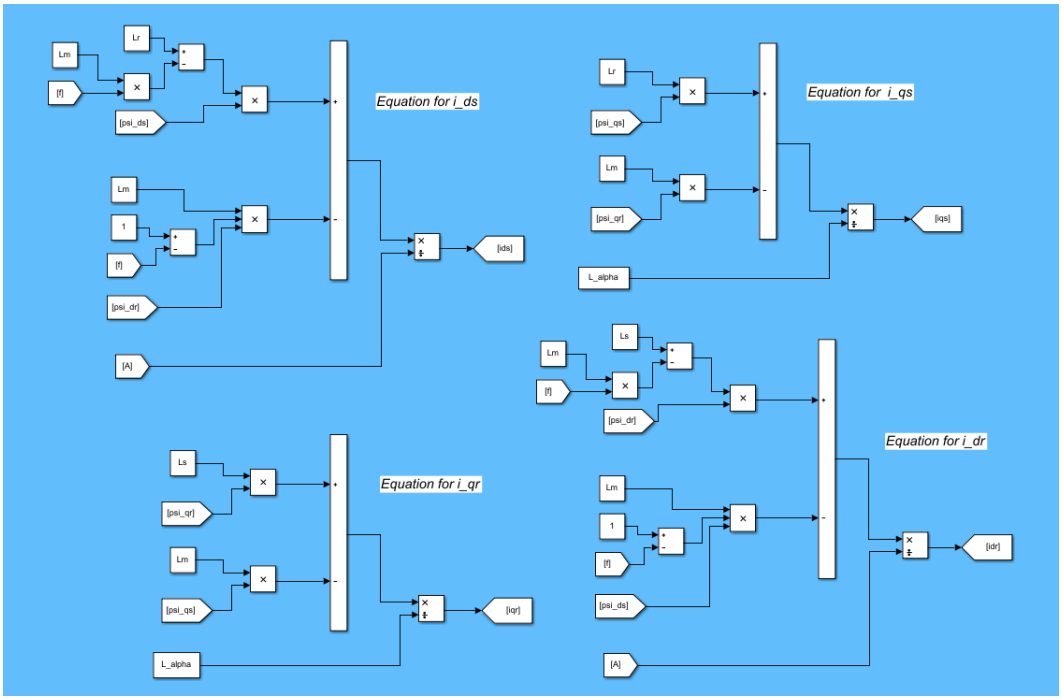

Figure 4.1.6: Voltage equation in dq frame for primary and secondary.

4.2 Modeling the controller

The previous section has motivated the selection of IFO vector control scheme for the current thesis problem. Therefore we start with modelling the current controller in the dq frame. Furthermore, we add a voltage saturation for limiting the reference voltage and use an anti-wind up method.

4.2.1 Clark and Park transformation

Before we proceed further, its worth discussing Clark and Park transformation. This transformation is used for transforming α β frame quantities into dq frame and vice versa. Generally it is common to have the current controller in the dq frame [2] while keeping the model in the α β frame. Thus in the block diagram the parameters of the motor model (voltage, current) are constantly transferred to and from dq frame to α β frame as they enter and leave the controller and the model block. The clark and park transformation can be seen in the Figure 3.2.1 as shown previously. The transformation is given as follows:

[2]The current controller is applied in a dq frame which synchronously rotates with motor flux .Therefore it allows using a similar control scheme as used in a DC motor

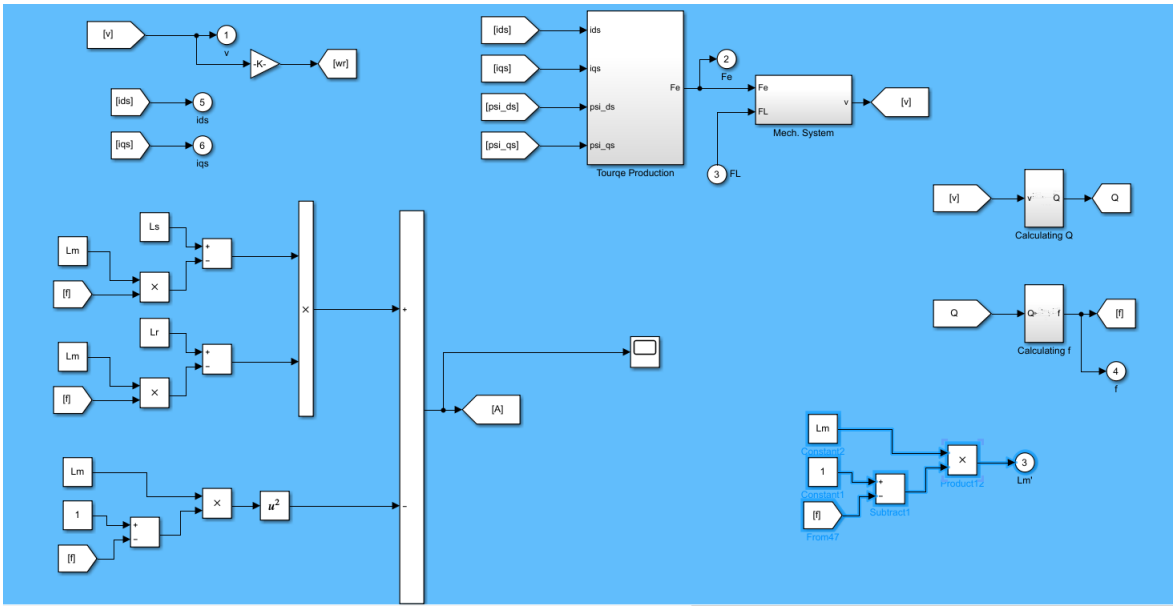

Figure 4.1.7: Additional equations for deriving the equivalent motor model.

$$\begin{bmatrix} x_d \\ x_q \end{bmatrix} = \begin{bmatrix} \cos\theta_1 & \sin\theta_1 \\ -\sin\theta_1 & \cos\theta_1 \end{bmatrix} \cdot \begin{bmatrix} x_\alpha \\ x_\beta \end{bmatrix}$$

Whereas its inverse *dq-frame* which is used to transform the parameter back to α β or motor frame and is given as:

$$\begin{bmatrix} x_\alpha \\ x_\beta \end{bmatrix} = \begin{bmatrix} \cos\theta_1 & -\sin\theta_1 \\ \sin\theta_1 & \cos\theta_1 \end{bmatrix} \cdot \begin{bmatrix} x_d \\ x_q \end{bmatrix}$$

Where x is the magnitude of the vector to be converted, while θ_1 is obtained by integrating ω_1 (angular voltage frequency) and is given as:

$$\omega_1 = \omega_r + \frac{\hat{R}_R i_q^{ref}}{\hat{\psi}_R} \tag{4.15}$$

$$\dot{\theta}_1 = \omega_1 \tag{4.16}$$

with (R_R) being the rotor resistance in case of RIM and secondary in case of LIM. However, it should be noted that in the current thesis work, we would refrain from using it since our controller is modelled in the dq frame directly and does not require transformation.

4.2.2 Current controller

Before we proceed to model the current controller, its important to understand the theory and dynamics behind it. The stationary frame model of an induction machine is given as [7]:

$$L\frac{d\mathbf{i}^s}{dt} = \mathbf{v}^s - R\mathbf{i}^s - \mathbf{E}^s \tag{4.17}$$

Such that

$$\mathbf{v}^s = \mathbf{v}_s^s \quad \mathbf{i}^s = \mathbf{i}_s^s \quad R = R_s \quad L = L_\sigma \tag{4.18}$$

where $\mathbf{v}_s^s, \mathbf{i}_s^s$ represents the stator (primary) voltage and current in the stationary $\alpha\ \beta$ frame whereas R_s and L_σ represents the stator (primary) resistance and magnetizing inductance respectively.

also

$$\mathbf{E}^s = \frac{d\boldsymbol{\psi}_R^s}{dt} \tag{4.19}$$

Given that $\mathbf{E}^s$ is derivative of the rotor (secondary) flux, we take $\mathbf{E}^s$ perpendicular to the dq frame such that

$$\mathbf{E}^s = jEe^{j\theta} \tag{4.20}$$

Thus based on the concept of synchronous coordinate transformation we can rewrite 4.17 in dq frame as following:

$$L\frac{d\mathbf{i}}{dt} = \mathbf{v} - (R + j\omega_1 L)\,\mathbf{i} - \underbrace{jEe^{j\tilde{\theta}}}_{\mathbf{E}} \tag{4.21}$$

Here, for modelling the controller we have assumed the behavior of LIM to be similar to that of a RIM, and have ignored the variation of Magnetizing inductance due to end effect.
Thus from 4.21 we have the following equations in d and q axis respectively.

$$L\frac{di_d}{dt} = v_d - Ri_d + \omega_1 Li_q - E_d \tag{4.22}$$

$$L\frac{di_q}{dt} = v_q - Ri_q - \omega_1 Li_d - E_q \tag{4.23}$$

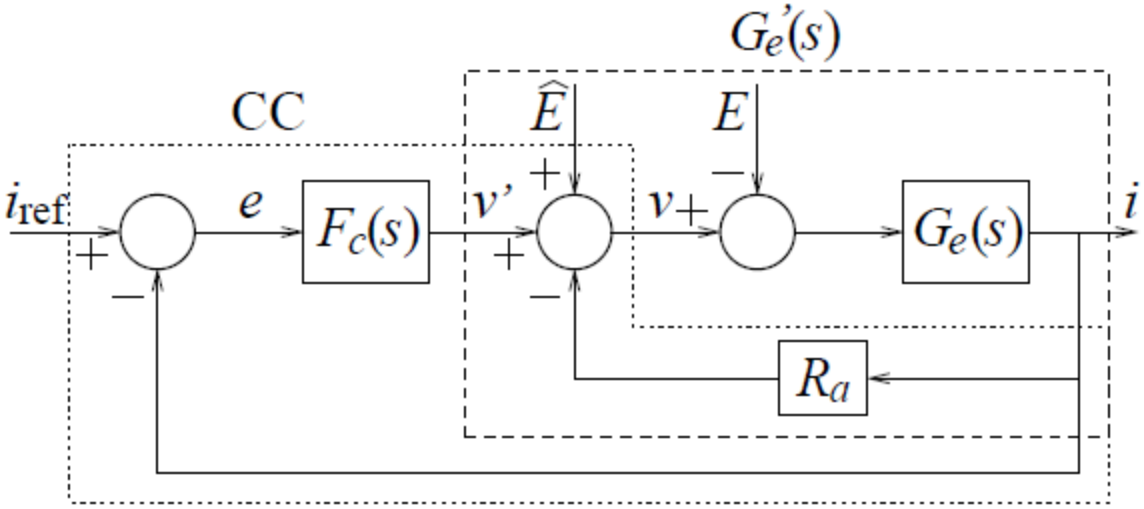

Figure 4.2.1: Two degree PI controller for DC Motor.

The above equations have two cross coupling terms in form of $\omega_1 L i_q$ and $\omega_1 L i_d$. The cross coupling terms should be removed in order to allow independent control of the d and q axis current component. At this point we dive first into the controller design for the DC motor, and take inspiration from it to subsequently use a similar strategy for the induction motor. Generally in DC motor due to load disturbance (caused by back emf generation) there is a steady state error. This error tends to be inversely proportional to the resistance of the motor. Therefore in order to improve the dynamics of the system and remove the steady state error an active resistance (R_a) which is a dummy resistance is added to the total resistance. This resistance is only present digitally and does not affect the power losses.
With the inclusion of active resistance R_a and feed forward of the back emf estimate $\hat{E}$ the controller obtained is a two degree PI controller with inputs as control error 'e' and current 'i'. Thus the electrical dynamics and control blocks are represented as shown in Figure 4.2.1 [7](Chapter 4)

In a control scheme similar to the one discussed above, it is possible to decouple the d and q terms by using active resistance. The transfer function **G**(s) obtained by applying laplace transform on 4.21 is given as 4.24

The cross coupling term jω_1L in 4.21 and 4.24 can be removed by adding a jω_1 $\hat{L}$ alongside the active resistance in the feedback loop. This gives the updated transfer

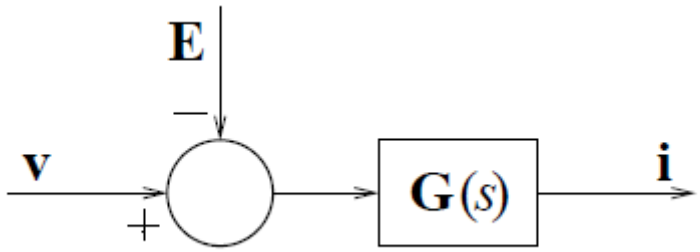

Figure 4.2.2: Block diagram for induction motor with transfer function **G**(s)

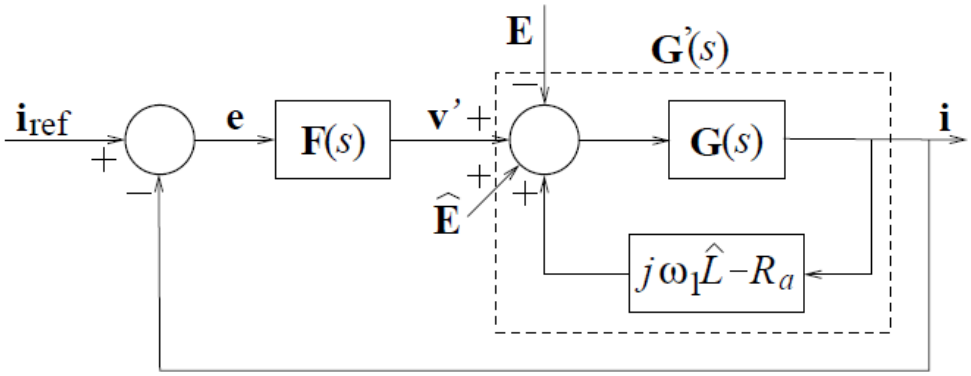

Figure 4.2.3: Two degree PI controller for 3 phase induction motor.

function **G'**(s) as shown in 4.25

$$\boldsymbol{G}(s) = \frac{1}{(s + j\omega_1)L + R} \tag{4.24}$$

$$\boldsymbol{G'}(s) = \frac{1}{sL + R + R_a} \tag{4.25}$$

Figure 4.2.2 and 4.2.3 [7]shows the block diagram of a 3 phase induction motor with open loop and a 3 phase induction motor with 2 degree PI closed loop controller. It is noted that the PI controller for induction motor in 4.2.3 resembles the PI controller for DC motor in 4.2.1 with only difference being the active resistance block. In Induction motor we have the additional decoupling term as discussed previously. Thus from 4.2.3 the transfer function from v' to i for the closed loop system is given as:

$$G'(s) = \frac{G(s)}{1 + (R_a - j\omega_1\hat{L})G(s)} = \frac{1}{sL + R + R_a} \tag{4.26}$$

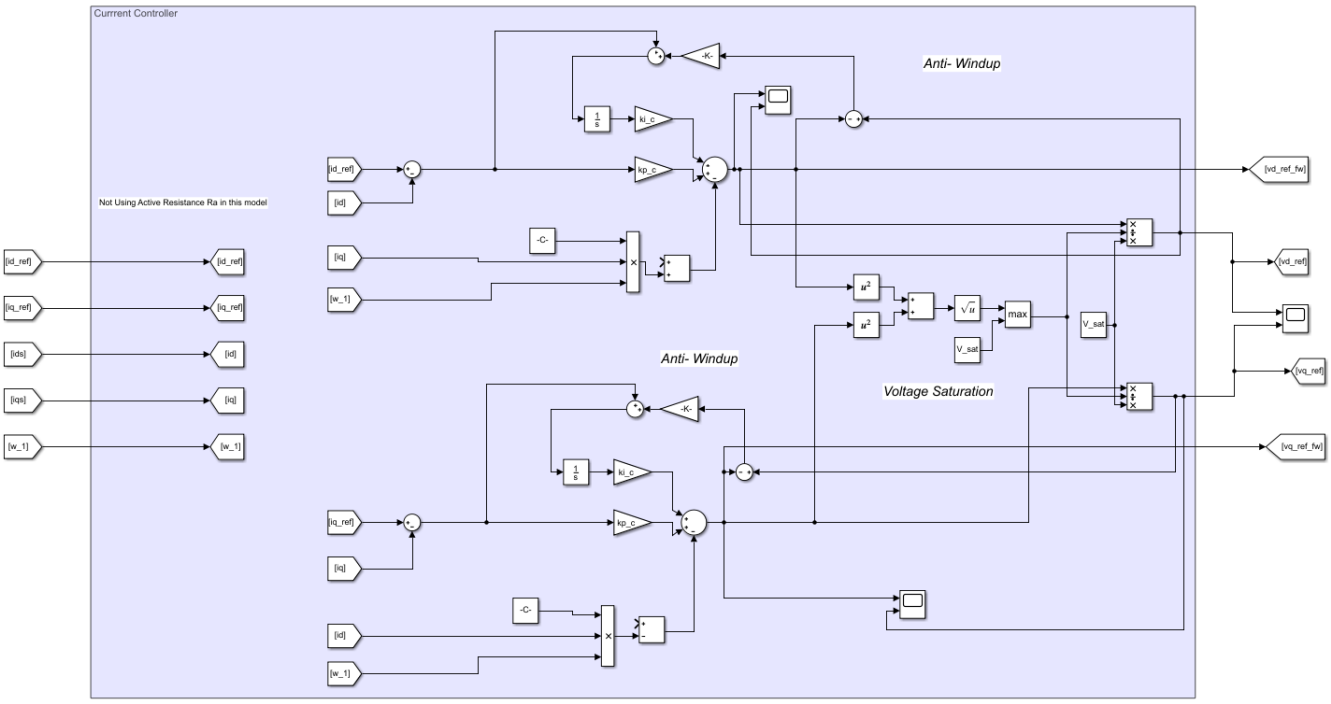

Figure 4.2.4: Simulink model of induction motor current control.

Hence by using direct synthesis we can obtain the controller parameter k_p and k_i as shown below:

$$F(s) = \frac{\alpha_c}{s} G'(s)^{-1} = \alpha_c \frac{sL + R + R_a}{s} = k_p + \frac{k_i}{s} \tag{4.27}$$

Here α_c is the desired bandwidth of the current controller.

$$\boldsymbol{F}(s) \cdot \boldsymbol{G'}(s) = \frac{\alpha_c}{s} \tag{4.28}$$

$$kp_c = \alpha_c \cdot \hat{L} \tag{4.29}$$

$$ki_c = \alpha_c \cdot (\hat{R} + R_a) \tag{4.30}$$

$$\hat{R} = R_\sigma = R_R + R_s \tag{4.31}$$

$$\hat{L} = L_\sigma \tag{4.32}$$

$$R_a = \alpha_c \hat{L} - \hat{R} \tag{4.33}$$

The final model of the current controller in simulink is shown as in Figure 4.2.4.

Here it should be mentioned that the control parameters have the same order as transient impedance $\boldsymbol{Z}_\sigma^s(s) = R_\sigma + s \cdot L_\sigma$. Also the sensitivity of the controller is much higher for variation in R_s when compared to R_R.

Moving forward, in order to set the reference value for the current controller we use equation 4.17 and 4.19 for getting i_d^{ref}. Whereas, for i_q^{ref} we set it arbitrarily [7].

$$\psi_R^{ref} = \sqrt{\frac{1 - L_\sigma^2}{1 + 2\frac{L_\sigma}{L_M}}} \tag{4.34}$$

$$i_d^{ref} = \frac{\hat{\psi}_R^{ref}}{\hat{L}} \tag{4.35}$$

Where $\hat{L}$ stands for the estimated magnetizing inductance and is equal to L_M.

4.2.3 Voltage saturation and anti wind up

In order to compensate for excessive high or low voltage request which is beyond the specified limit of V_{base} we use the voltage saturation block. It limits the magnitude of supplied voltage in v_d and v_q to the maximum voltage of V_{base}. Generally the output voltage from current controller can exceed V_{base} when their is a sudden large steps in i_{ref}. The saturation limit act as a guard for protecting the power electronic components from getting higher voltage supply than rated. The voltage saturation block in the simulink model is shown in Figure 4.2.5.

Another interesting aspect of the current controller is the anti-windup configuration. Integrator wind up occurs when there is a huge gap between the set point of the controlled parameter and the actual value (error), which gets accumulated due to the integrator part of the controller. In a motor it can occur when the voltage has reached its saturation limit while the current request is still active.
An anti-windup, (as the name suggests) stops the system from getting wound-up and have an overshoot. The anti-windup method used here is called 'back calculation' where a modified control error is introduced to the integrator side of the controller. The modified control error $\bar{e}$ is selected as such that the motor never enters the saturation region and is given as 4.36[7]

$$\bar{e} = e + \frac{1}{k_p} \cdot (\bar{v}_{ref} - v_{ref}) \tag{4.36}$$

Here e stands for the control error and $\bar{e}$ for the modified error. k_p represents the proportional gain, $\bar{v}_{ref}$ is the actual (saturated) voltage reference and v_{ref} is the ideal voltage reference. This method is called back calculation since it uses the value of $\bar{v}_{ref}$

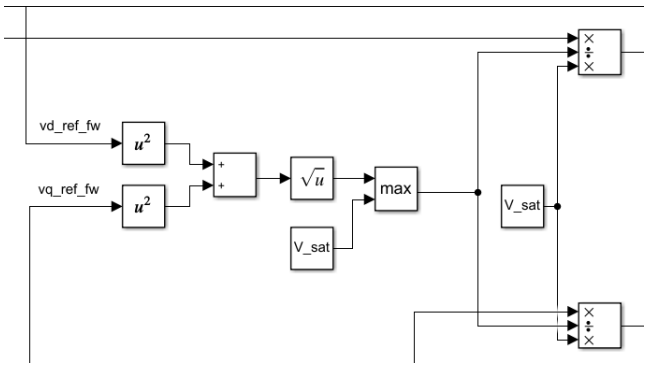

Figure 4.2.5: Voltage saturation block.

to calculate the corresponding value of $\bar{e}$ avoiding intergrator wind up.

Thus the control equations including back emf calculation are shown as following:

$$e = i_{ref} - i \tag{4.37}$$

$$\frac{d\boldsymbol{I}}{dt} = \bar{\boldsymbol{e}} \tag{4.38}$$

$$\boldsymbol{v}_{ref} = kp_c\boldsymbol{e} + ki\boldsymbol{I} + (j\omega_1\hat{L} - R_a)i + \hat{\boldsymbol{E}} \tag{4.39}$$

$$\bar{\boldsymbol{v}}_{\boldsymbol{ref}} = Sat(v_{ref}, V_{base}) \tag{4.40}$$

4.3 Current model

It is difficult to measure the motor flux directly, thus the lack of accuracy in measurement makes motor model unreliable and not to mention it also adds up to the total cost of the motor. Hence, it is more suitable to use a flux estimator for estimating the motor flux. Here we are considering the flux estimation bu using a model called 'Current Model'.

The current model is implemented assuming perfect field orientation and uses the same set of equation as discussed previously in section 3.2.2. Thus equations 3.3, 3.4 and 3.5 are used to derive the 'Current Model' as shown in 4.2.5. It should be pointed out that the 'current model' uses the dynamic equation for a RIM and not for a LIM. Hence the the magnetizing inductance remains constant and is not a variable.

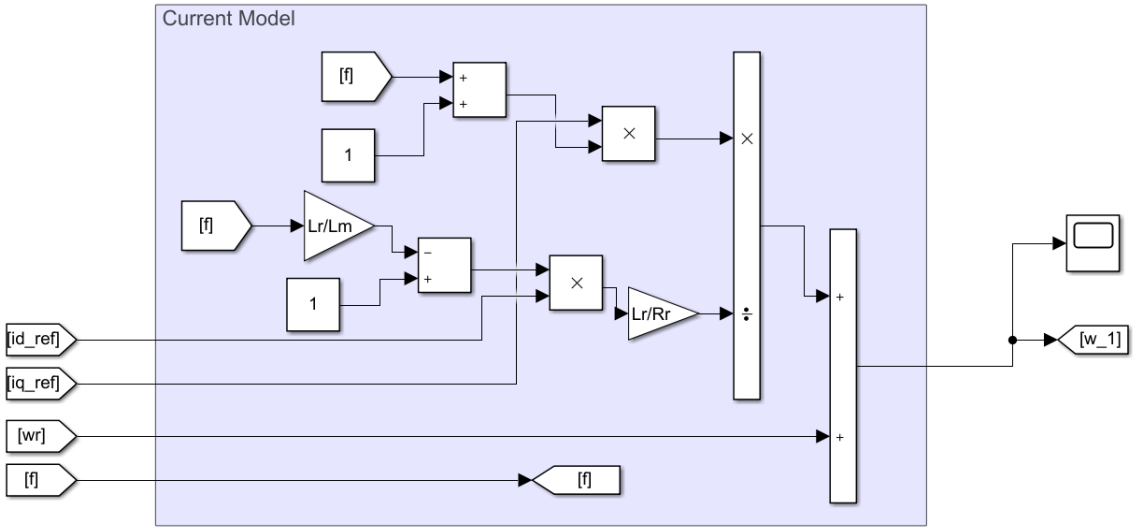

Figure 4.3.1: The 'current model' as modelled in simulink.

4.4 Speed controller

So far we have focused mostly on the electrical dynamics of the motor, but here we shift our attention to the mechanical dynamics/speed of the motor. Implementing a speed controller means trying to control the q axis component of current which controls the torque(or thrust in LIM) and thus in turn the speed.

Moreover it should be noted that the speed controller is the outer loop (while the current controller is the inner loop) of the cascaded control structure used for controlling the induction motor.Hence the response dynamics of speed controller differs from and is dependent on the inner loop response dynamics of current controller.

However if we look into the individual control dynamics of the speed and the current controller they seem analogous to each other with i_q^{ref} being the output of the speed controller. The analogy is further seen in the effect of load disturbance in the mechanical dynamics similar to the the back emf in current controller. So a strategy similar to active resistance in current controller is used in speed controller in form of active viscous damping. The mechanical dynamics with active damping b_a is thus represented as 4.41 [7]:

$$\frac{d\omega_r}{dt} = \frac{\psi}{J}(i' - b_a\omega_r) - \frac{b}{J}\omega_r - \frac{\tau_L}{J} \tag{4.41}$$

Here τ_L is the external load torque independent of speed whereas $b\omega_r$ is the speed

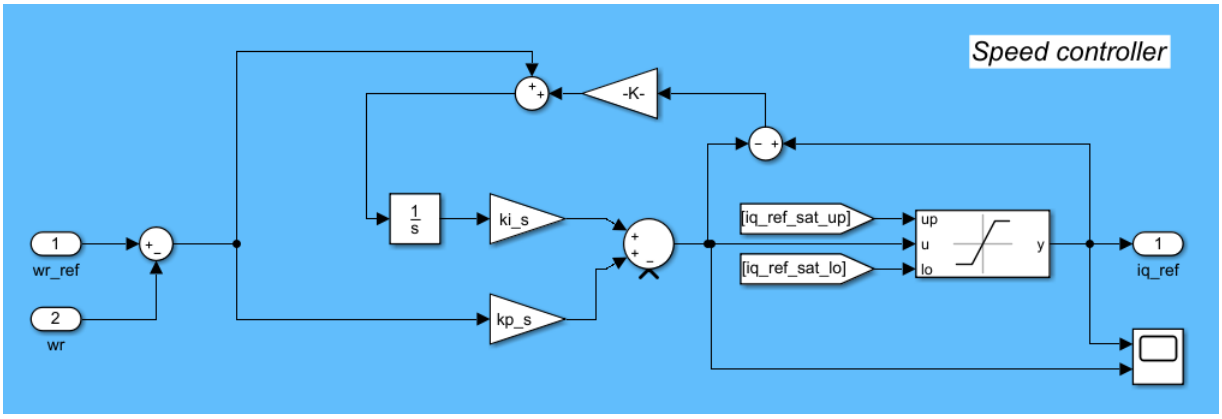

Figure 4.4.1: The Speed controller as modelled in simulink

dependent external torque load component. The term i' shows the inclusion of active viscous damping for improving system's dynamics such that $i = i' - b_a\omega_r$.
If,

$$b_a = \frac{\alpha_s \widehat{J} - \widehat{b}}{\widehat{\psi}} \tag{4.42}$$

where α_s is the desired bandwidth of the speed controller. Then accordingly the transfer function $\boldsymbol{G}(s)$ for 4.41 is given as following We use the principal of direct synthesis (used previously for current controller) to determine the corresponding values of controller parameter as shown below [7](chapter 4):

$$\boldsymbol{G}(s) = \frac{\frac{\hat{\psi}}{\hat{J}}}{s + \alpha_s} \tag{4.43}$$

$$\boldsymbol{F}(s) \cdot \boldsymbol{G}(s) = \frac{\alpha_s}{s} \tag{4.44}$$

$$kp_s = \frac{\alpha_s \hat{J}}{\hat{\psi}} \approx \frac{\alpha_s \hat{J}}{\psi_{ref}} \tag{4.45}$$

$$ki_s = \frac{\alpha_s^2 \hat{J}}{\hat{\psi}} \approx \frac{\alpha_s^2 \hat{J}}{\psi_{ref}} \tag{4.46}$$

$$\hat{b}_a = \frac{\alpha_s \hat{J} - \hat{b}}{\hat{\psi}} \approx \frac{\alpha_s \hat{J} - \hat{b}}{\psi_{ref}} \tag{4.47}$$

$$\tag{4.48}$$

The improved dynamics response by introducing the active viscous damping constant b_a is such that the inner feedback loop and outer close loop are equally fast. Also the speed control is designed in a way such that the current control is 120 times faster than it.

4.5 Field weakening controller

It is common to demand from an induction motor a speed greater than the base speed during its operation. In an induction machine this is made possible by a special type of controller referred to as field weakening or flux weakening controller. As the name suggests the controller tries to reduce the flux when the motor is requesting a speed greater than the base speed. Since power is a product of torque and angular speed (here thrust and linear velocity) which becomes constant after reaching its maximum value at the maximum torque and base speed, hence in order to increase the speed further the torque needs to be reduced to respect the power limits. Reduction of torque means reduction of secondary (rotor) flux since torque and flux are directly proportional to each other.

Thus the controller is designed in order to reduce the current component i_d which controls the flux. We get the following expression 4.51 as seen [7]

$$i_d^{ref} = k_{fw} \int [V_{base}^2 - (v_d^{ref})^2 - (v_q^{ref})^2] \text{ dt } |_{I_{min}}^{I_{nom}} \tag{4.49}$$

$$I_{nom} = \frac{\psi_{ref}}{\hat{L}_M} \tag{4.50}$$

$$I_{min} = 0.1 I_{nom} \tag{4.51}$$

It should be noted that the gain value k_{fw} is selected in a way that it does affect the field below the base speed. Thus we have 4.52 representing the gain k_{fw} as

$$k_{fw} = \frac{\hat{R}_R}{\hat{L}_{sigma}^2 V_{base} max(|\omega_1|, \omega_{base})} \tag{4.52}$$

Here V_{base} represents the base voltage,I_{nom} is the nominal current, I_{min} is the minimum current while v_d^{ref} and v_q^{ref} are the voltage components in the dq frame, and act as reference input for the inverter. The field weakening region is divided into two regions. This division depends on the conditions leading to maximum torque generation. If the maximum torque is obtained by applying nominal current, the field weakening is said to be present in region 1. However, if the maximum torque is obtained for a current lower than the nominal current for a certain primary (stator for RIM) frequency then it is said to be in region 2.

In order to operate in region 2, we use the relation as shown in Equation 4.54 where we aim at reducing the q component of the current

$$i_q^{ref} = \text{sat}\,[i_{q,nom}^{ref}, \min(\sqrt{I_{max}^2 - (i_d^{ref})^2}, \zeta i_d^{ref})] \tag{4.53}$$

$$\zeta = \frac{\hat{L}_\sigma + \hat{L}_M}{\hat{L}_\sigma} \tag{4.54}$$

The controller parameter is shown above in 4.45, 4.46 and 4.47. The actual field weakening control parameter is modified to accommodate for ψ_{ref} which is used in the development of the speed controller. It is also noted that in the current study active viscous damping has not been used hence we neglect $\hat{b}_a$ or make it equal to zero.

4.6 Model overview

In the previous sections we have modelled the individual systems namely, the LIM motor model, the current controller, the speed and field weakening controller and the 'current model'. In this section we explain briefly how the different systems are working together. The overview of the system is shown in Figure 4.6.1. The system comes in action with a demanded speed request in the speed controller. The speed controller thus in turn calculates the value of i_q^{ref} in the outer loop and feeds it to the current controller. In the meantime the speed controller block having the field weakening algorithm within it also calculates the value of i_d^{ref} as an input to the current controller. The current controller having the reference input current generates the corresponding output voltage v_d^{ref} and v_q^{ref}. It should be noted that the current controller block also contains the voltage saturation and anti wind up algorithm. The generated voltage references are then fed into the LIM model which finally gives the developed speed and thrust force from the motor. The corresponding values of current and flux in d and q axis from the motor are fed into the respective controller for in turn calculating their output. Throughout this time the current model estimates the motor flux and thus give the value of ω_1.

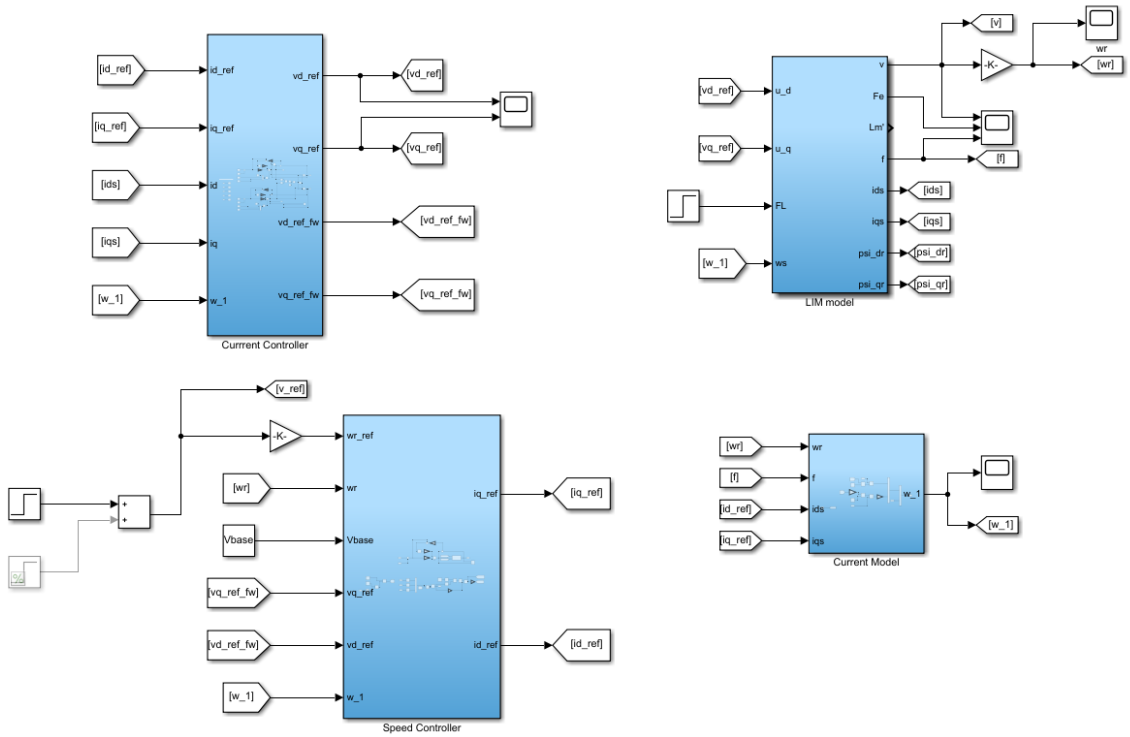

Figure 4.6.1: Overview of entire modelling.

Chapter 5

Analysing the results

The results of the current study with respect to the designed controller and motor model are discussed in this section. It is important to point out the deliminator for the current study one more time. Since the controller relies heavily on the motor electromagnetic parameter, it is crucial to measure them accurately.
Due to a subsequent change in the track length for the competition (by SpaceX) the motor design has to undergo drastic changes. Since the new motor design was still in development and the old design was never manufactured, no testing was done to determine the correct and reliable motor parameters.
Hence the study is continued forward by using the subsequent motor parameter from [11] especially for the electromagnetic parameters. The table below summarises the parameters used for deriving the results of this study. The same has been described in

Table 5.0.1: Motor parameters.

Parameters	**Values**
Motor rating	7.50 KW
Primary resistance	1.29 ohm
Secondary resistance	0.975 ohm
Primary Inductance	0.0684 H
Secondary Inductance	0.0416 H
Magnetising Inductance	0.0416 H
No. of poles	4
Length of Primary	1m
No. of poles	4

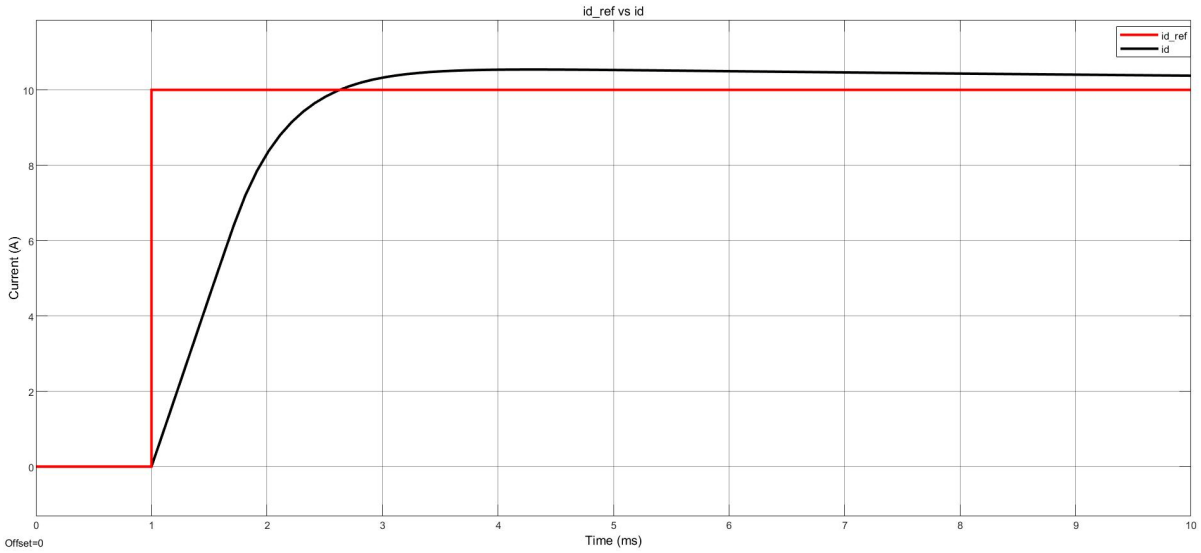

Figure 5.1.1: Variation of i_d with respect to i_dref for zero load.

the Matlab script attached in the appendix.

5.1 Current controller

We start by describing the response of the current controller for the designed motor model. As discussed previously it is important to remember that the end effect has been incorporated in the motor model but not in the current model. The response of the current controller for a step reference of i_d and i_q current of 10A and constant frequency 25 Hz (half of base frequency) can be seen in Figures 5.1.1 and 5.1.2 for d and q primary (stator) current respectively. The rise time is in the orders of 1ms. It can also be observed that there is an over and under shoot for the i_d and i_q current respectively. Moreover this error remains as a steady state error in both the components. This behavior can be attributed to the lack of field weakening parameter in the current controller. Since the end effect forces the magnetic inductance to become a variable, whereas in the current controller the magnetic inductance has been taken as a constant. This directly affect the controller response and results in the steady state error.

5.2 Load conditions

Moving forward, the other key aspect of the control strategy is to accommodate the load requirement on the motor and allow field weakening that is to get higher speed than at the nominal value, while decreasing the flux accordingly. The ideal solution will be to

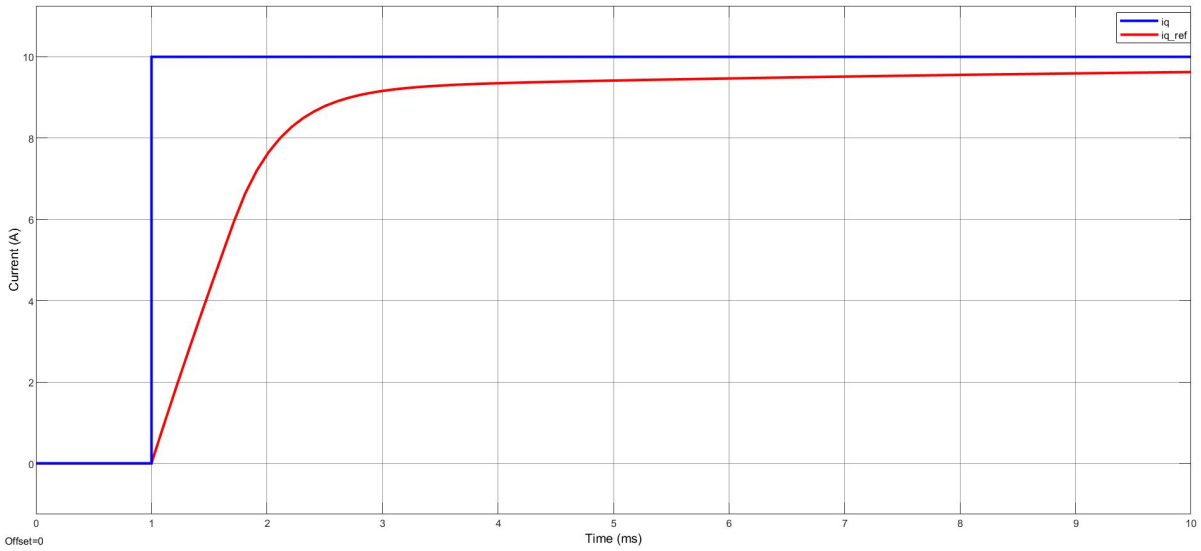

Figure 5.1.2: Variation of i_q with respect to i_{qref} for zero load.

get a torque vs velocity profile, in our case thrust vs. velocity profile for the designed motor for achieving a target reference speed. However, due to lack of motor parameters as stated previously and subsequent use of parameters from previous literature we have modified the motor capacity. Hence we restrict ourselves to the small step input load values. Thus keeping that in mind we simulate different load cases to verify that our control algorithm as well as the model works as expected. We start with three load cases 5N, 50N and 500 N respectively with a reference velocity of 20m/s.The reference velocity as well as the load forces are entered as a step input with a step time of 1 second and 1.5 seconds respectively. The step time of the reference velocity is always selected as smaller since this gives motor time to energise in advance.

5.2.1 Load=5N

The results for the first condition that is a load force of 5N and a velocity reference of 20m/s is discussed in this section.

In Figure 5.2.1 we observe how the controller controls the linear velocity to match the reference step velocity of 20m/s. There is no overshoot and the steady state error is zero. The rise time is 0.45 which is slow (compared to the expected value of 0.1 second) but acceptable for the mechanical dynamics.

Figure 5.2.2 represents the variation of current i_d and i_q for the primary of the LIM. It is seen that the current in i_d and i_q settles down to a constant value of 15 and 0 respectively. However there is a transient drop and increase in i_d and i_q at around 1.5

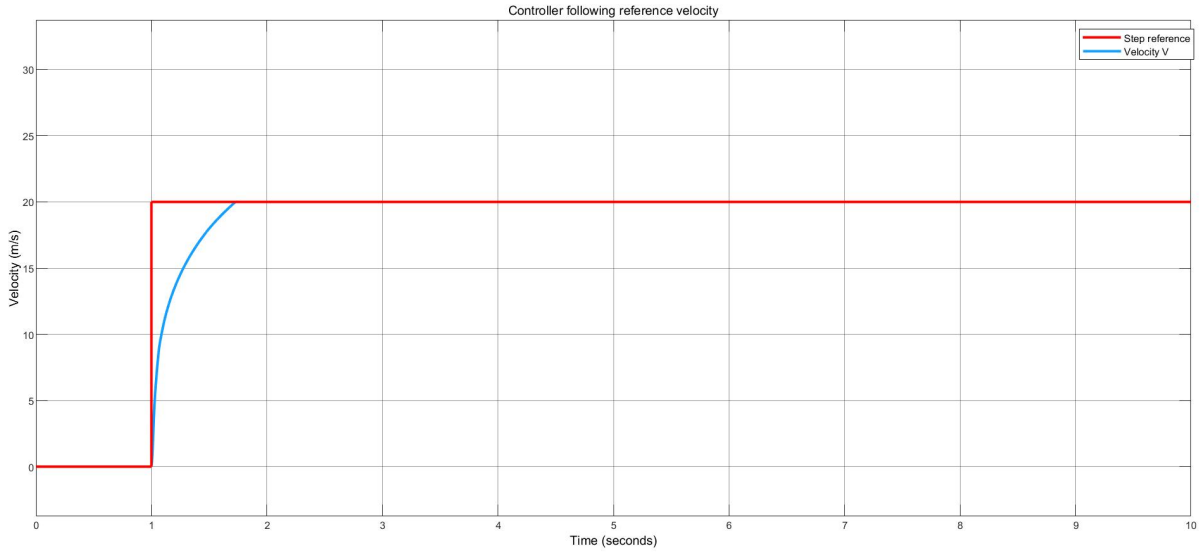

Figure 5.2.1: Reference velocity and linear velocity (5N).

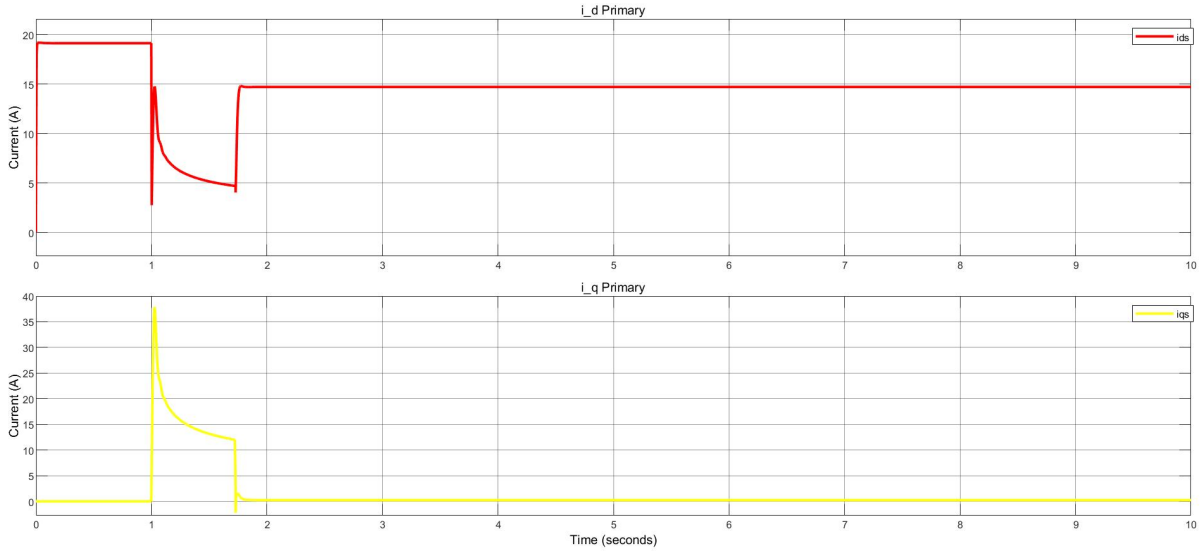

Figure 5.2.2: Variation of current in i_d and i_q (5N).

second which is attributed to the applied load.

The variation of magnetic flux for the secondary along i_d and i_q axis is shown in Figure 5.2.3. In addition to that that the total magnitude of the flux is also represented. It is seen that the flux in d axis first increases then decreases and settles down to a constant value. Whereas the flux in q axis is tending to zero with a transient decrease in the beginning. This observed behavior is due the perfect field orientation and in a way verifies the modelling.

Figure 5.2.4 represents the variation of the linear velocity, thrust force and end effect parameter. The linear velocity matches the reference velocity of 20m/s. It is also seen that the thrust force peaks at 2400N and then finally settles down to the load force of

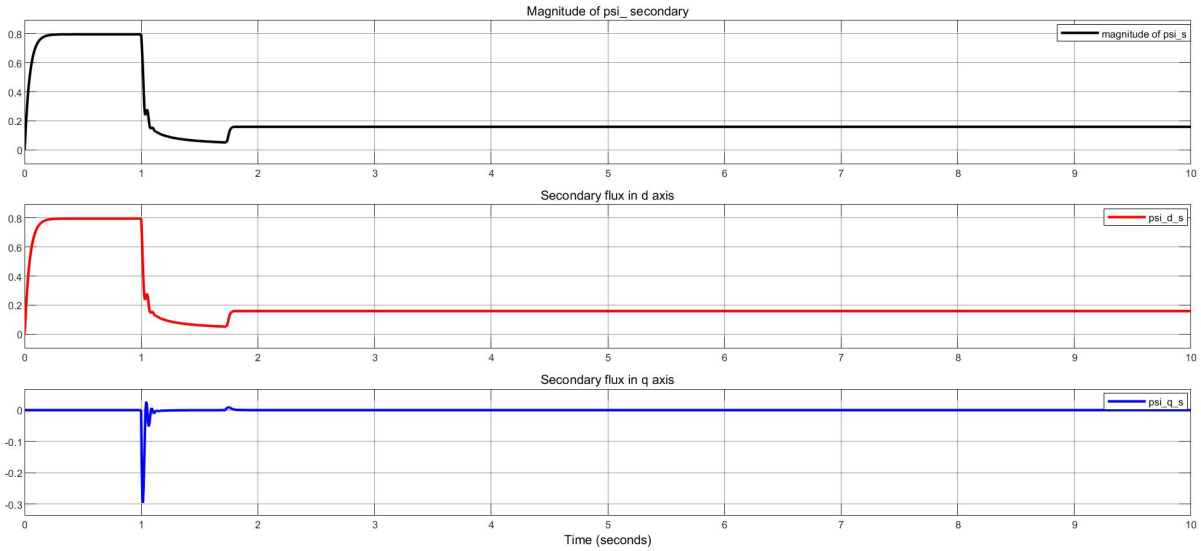

Figure 5.2.3: Variation of magnetic flux in i_d and i_q axis (5N).

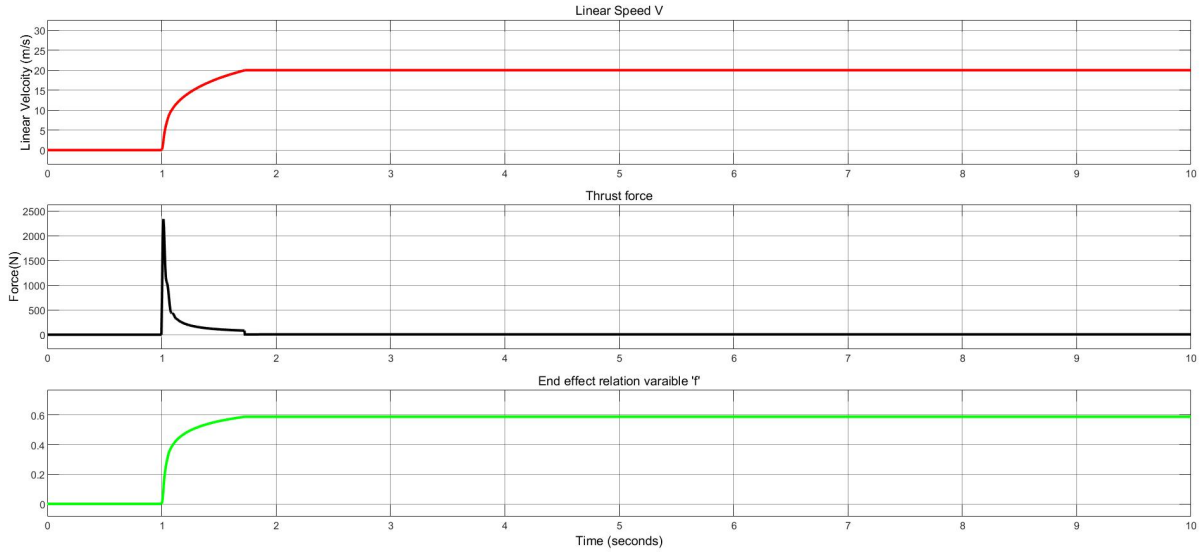

Figure 5.2.4: Variation of thrust force, linear velocity and end effect parameter (5N).

50N. Whereas the value of 'f' tends to 0.6.

5.2.2 Load= 50N

This section discusses the results for the load value of 50N.

Figure 5.2.5 represents the response of speed controller. The speed controller is able to track the input reference velocity. No overshoot and steady state error is seen. However, there is a slight increase in the rise time when compared to a load value of 5N. The rise time increases from 0.45 second to 0.47 second.

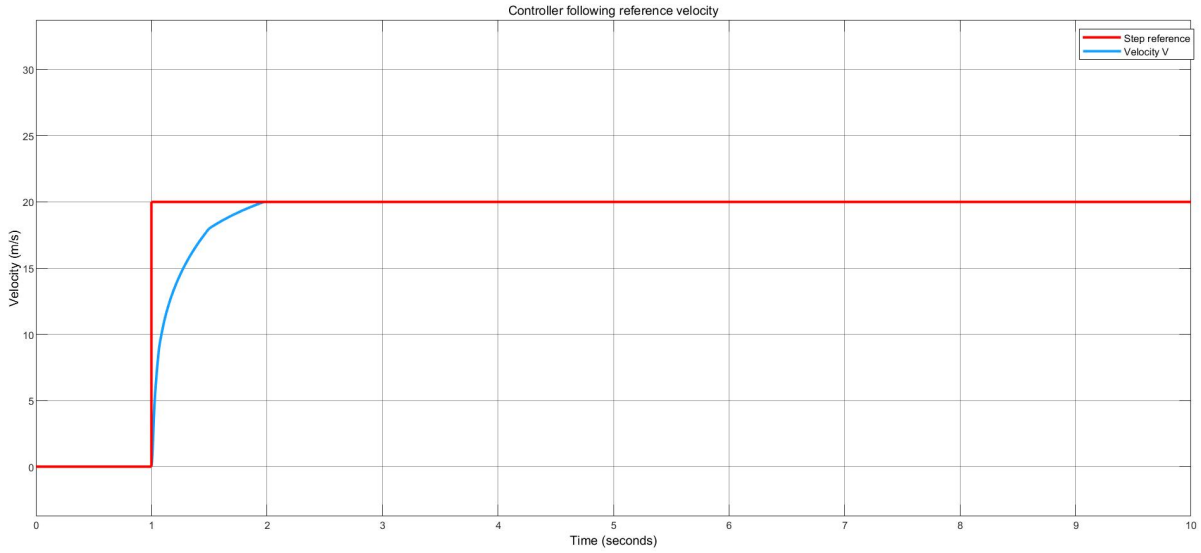

Figure 5.2.5: Reference velocity and linear velocity (50N).

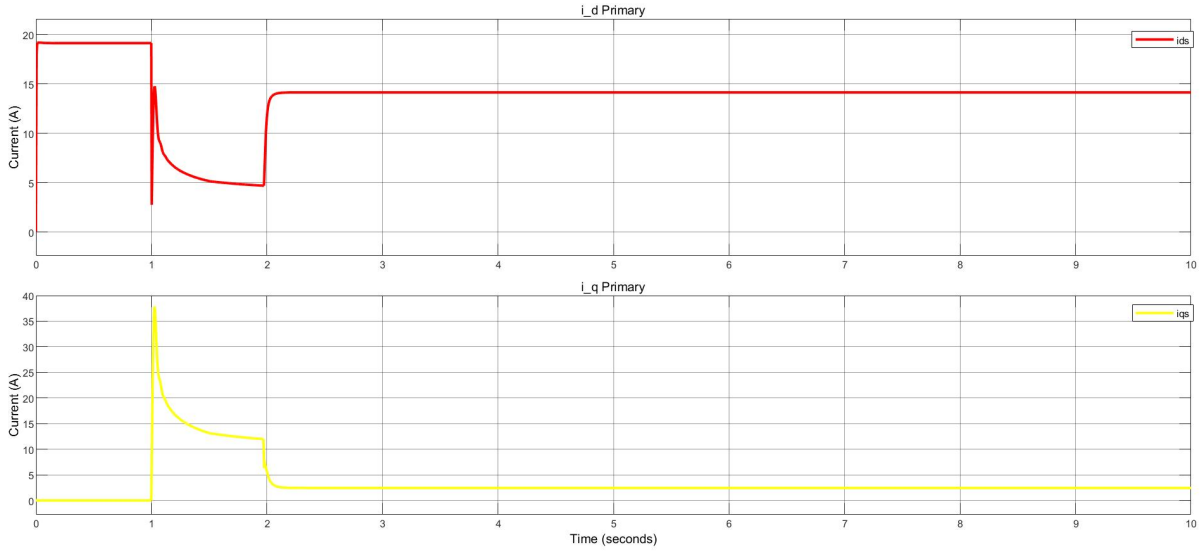

Figure 5.2.6: Variation of current in i_d and i_q (50N).

In Figure 4.46 the variation of the current in d and q axis is shown respectively for a load value of 50N. The profile looks similar to that of 5N load force. However with 50N of load force the i_d current settles at a lower value of 14.1 A when compared to 15A for 5N load case. Moreover, the i_q current settles for a higher value of 2.4A, when compared to 0A for 5N load case. This behavior can be attributed to the motor's operation in the field weakening region 1.

The variation of the magnetic flux for the load value of 50N is shown in Figure 5.2.7.

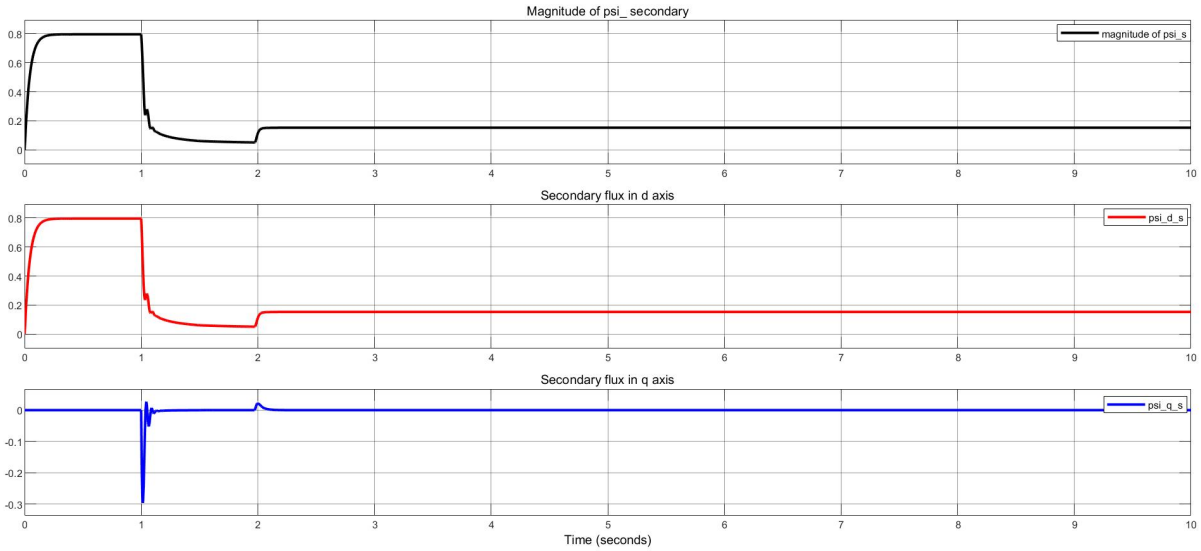

Figure 5.2.7: Variation of magnetic flux in i_d and i_q axis (50N).

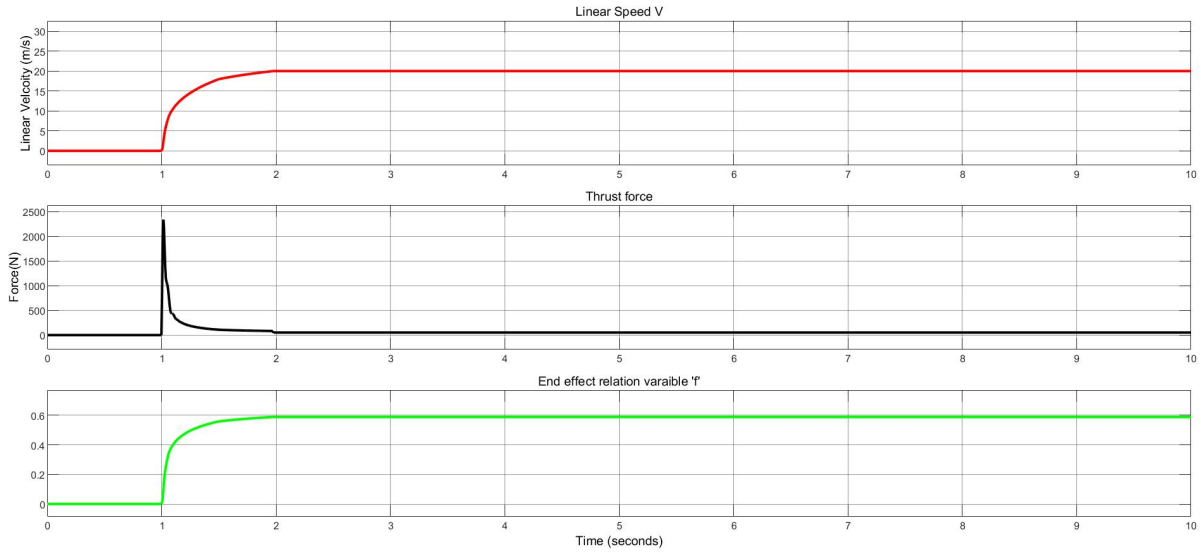

Figure 5.2.8: Variation of thrust force, linear velocity and end effect parameter (50N).

The profile is similar to that of the 5N load case. Moreover, the values are similar with very minor deviations. The figure represent perfect field orientation as the flux in q axis remains zero (except some transient response in the beginning).

Whereas the thrust force and end effect parameter 'f' is represented in Figure 5.2.8. The response is similar to that of 5N load force, with almost zero deviation between both the cases.

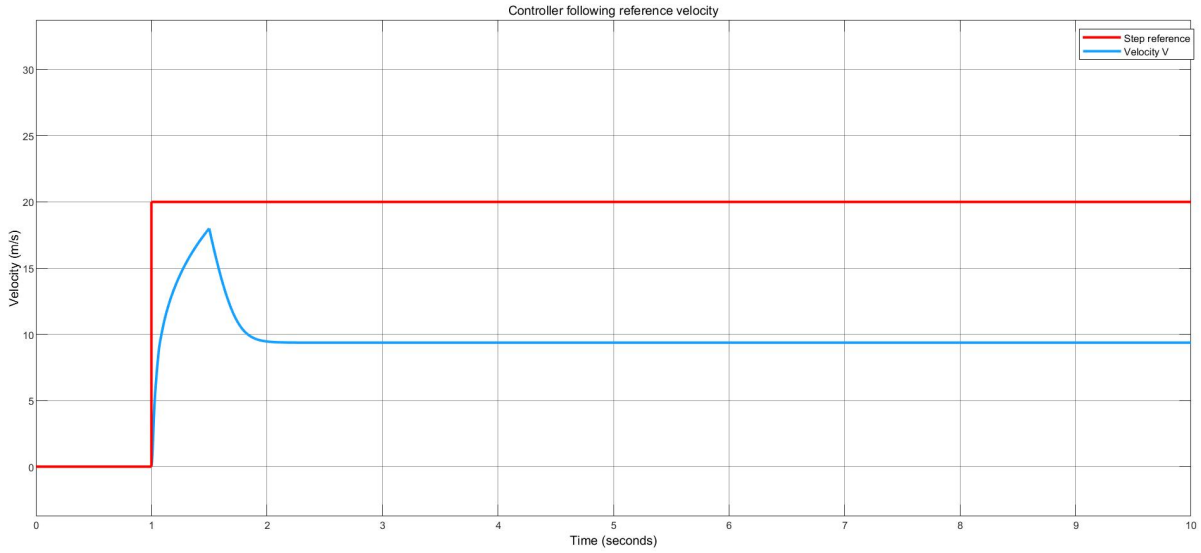

Figure 5.2.9: Reference velocity and linear velocity (500N).

5.2.3 Load= 500N

In this section we discuss the results for the load value of 500N.
Figure 5.2.9 shows the response of the controller to the reference velocity step input of 20m/s. The controller fails to reach the reference velocity as seen in the figure, and settles down at 9m/s. This behavior is attributed to the operation of the motor in the filed weakening region 2. The velocity increase is restricted to the maximum power rating of the motor which is 7.5 KW.

In Figure 5.2.10 the variation of i_d and i_q current is shown. The value of i_d is significantly less when compared to the other two load cases previously. Whereas the value of i_q is significantly higher compared to the the previous load cases. This means the motor is operating in the field weakening region and hence the i_d decreases allowing i_q to increase subsequently.

The variation of magnetic flux as seen in Figure 5.2.11 suggests that the q axis flux settles down to zero giving perfect filed orientation, this response is similar to the previous load cases that were discussed. While in Figure 5.2.12 the variation of thrust force and end effect parameter 'f' for 500N load is shown. The maximum thrust force generated is still 2400N, while the thrust force settles down to a constant value of 500N as demanded through the load force. This in turn validates the motor model developed in the study. The value of 'f' is smaller when compared to the value obtained in previous loading condition. This is attributed to the dependency of the duncan parameter Q which in turn depends on the velocity. Since the steady state Velocity in this case is

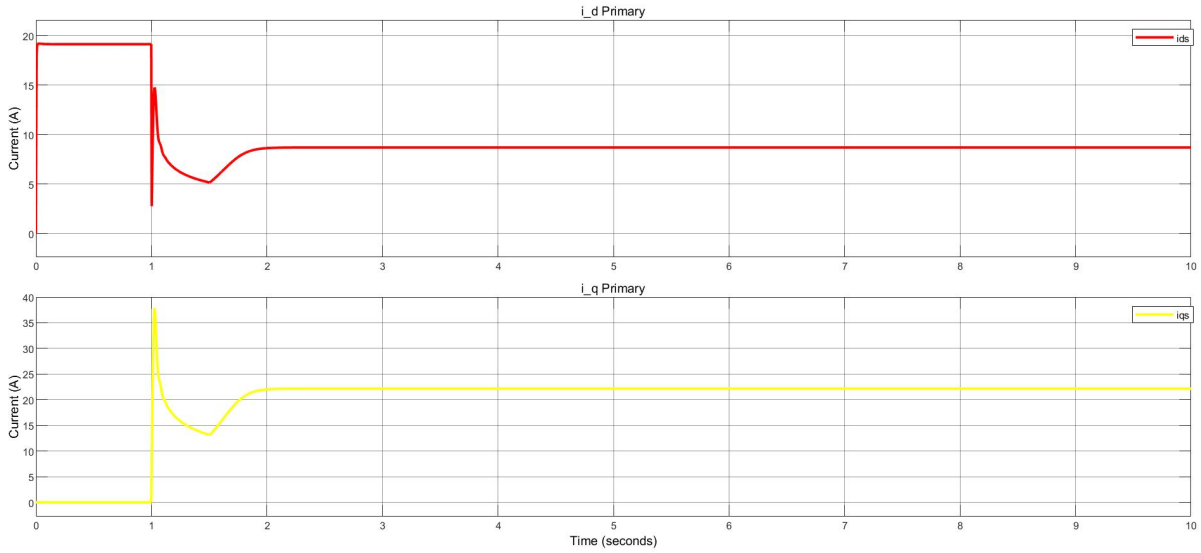

Figure 5.2.10: Variation of current in i_d and i_q (500N).

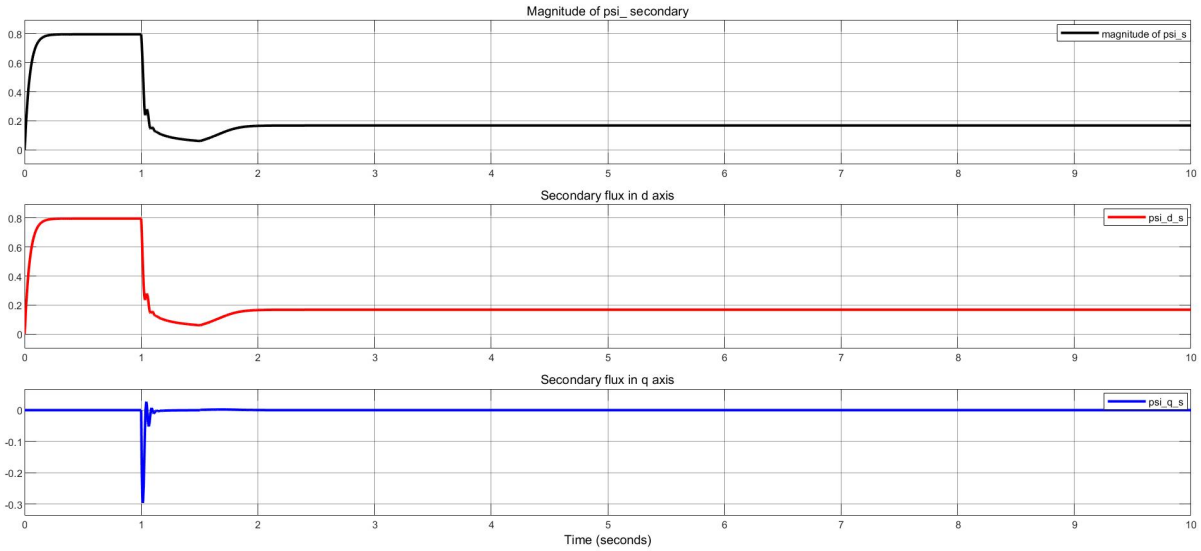

Figure 5.2.11: Variation of magnetic flux in i_d and i_q axis (500N).

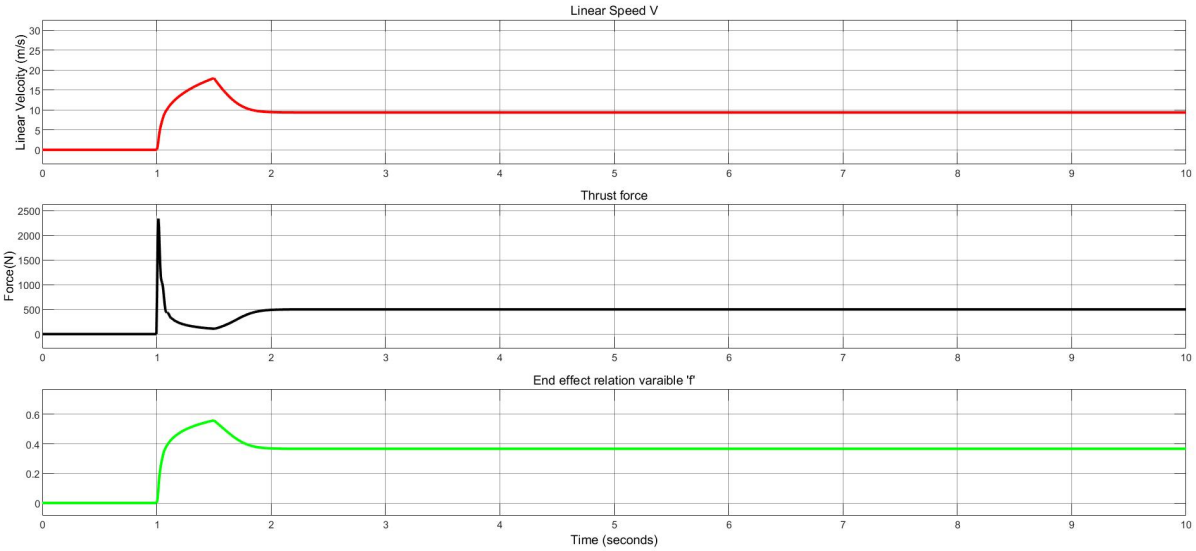

Figure 5.2.12: Variation of thrust force, linear velocity and end effect parameter (500N).

about 9m/s we see a corresponding decrease in the value of Q and f.

Chapter 6

Conclusions

6.1 Discussion

The main objective of this thesis was to simulate and build a motor model and a corresponding controller which can be used to control a double sided Linear induction motor to achieve a target velocity. Therefore the study started by reading the existing literature and to develop a better understanding of induction motor control. In order to begin with modelling related articles and modelling methods were studied for a RIM, which was later used as a stepping stone to model and understand the development of LIM. Different control methods were studied, investigated and compared for their practicality, ease of implementation and robustness. After developing an understanding of RIM, the LIM model was bench marked against it and the major difference between the two i.e, the presence of end effect in LIM was identified and accommodated in modelling.

Once the motor was modelled, the next step involved designing the controller. The controller was developed step by step, starting with a current controller to control the electrical dynamics followed by inclusion of a current model for estimation of the magnetic flux and then finally modelling the speed controller together with a field weakening controller to allow control of velocity in field weakening regions.

Since the problem was highly dependent on delimitation from lack of motor parameters, a previous research work was used for getting those parameters. This has turned out to be one of the improvement points /future work for the current study in order to meet the thesis goal. In addition to that the current controller does not accommodate the variable magnetic inductance produced due to the end effect but

instead uses a constant value of magnetizing inductance. This is another improvement work for meeting the goal of the thesis.
In totality however the thesis is able to produce a solution to start off with, for the given problem. The designed model and the controller seems to work good enough to achieve a target reference speed for an applied step load. Nevertheless due to limited time, the complexity of the thesis topic and uncertainty regarding model parameters the scope of the thesis has been reduced and some of the improvements are suggested in the next section of future work.

6.2 Future work

As discussed in previous section even though a decent portion of the thesis goal has been achieved, there still lies a scope for improvement. Given the inter-dependency of the thesis work on parameter estimation and a strong theoretical pre-requisite it was difficult to achieve all the goals in the allocated time, hence following future works are suggested:

- Estimation of the motor parameter for the scaled hyperloop pod: Since in the current study due to design modifications and updates the motor parameter has not been measured or estimated. So a suggestion would be to add stationary testing for determining these parameters.
- Inclusion of end effect in the controller modelling: In order to improve the accuracy of the controller, it is advised to accommodate the end effect variation in the controller model.
- Addition of inverter model: The current study does not include the actual implementation through an inverter model. Therefore one of the important addition would be to add an inverter model and have a discretized control for an actual implementation.

6.2.1 Final words

The thesis work has managed to achieve most of its objective, but one main objective of using the developed motor model and the corresponding controller for the actual scaled hyperloop LIM requirement has not been met. However once the electromagnetic parameter identification for the LIM is done and the desired load profile as a function

of velocity is obtained the developed thesis model could be used to verify the response of the model and controller without any difficulty.

Bibliography

[1] Bessaih, Brahim, Boucheta, Abdelkrim, Bousserhane, Ismail Khalil, Hazzab, Abdeldjbar, and Sicard, Pierre. “Speed control of linear induction motor considering end-effects compensation using rotor time constant estimation”. In: *International Multi-Conference on Systems, Signals & Devices*. IEEE. 2012, pp. 1–7.

[2] Caruso, M, Cipriani, G, Di Dio, V, Miceli, R, and Spataro, C. “Speed control of double-sided linear induction motors for automated manufacturing systems”. In: *2014 IEEE International Energy Conference (ENERGYCON)*. IEEE. 2014, pp. 33–38.

[3] Duncan, J. “Linear induction motor-equivalent-circuit model”. In: *IEE proceedings B-electric power applications*. Vol. 130. 1. IET. 1983, pp. 51–57.

[4] Hughes, Austin and Drury, Bill. *Electric motors and drives: fundamentals, types and applications*. Newnes, 2019.

[5] Kang, G and Nam, K. “Field-oriented control scheme for linear induction motor with the end effect”. In: *IEE Proceedings-Electric Power Applications* 152.6 (2005), pp. 1565–1572.

[6] Krause, Paul C, Wasynczuk, Oleg, Sudhoff, Scott D, and Pekarek, Steven. *Analysis of electric machinery and drive systems*. Vol. 2. Wiley Online Library, 2002.

[7] Lennart Harnefors, Marko Hinkkanen and Wallmark, Oskar. “Control of Voltage-Source Converters and Variable-Speed Drives”. In: *Control of Voltage-Source Converters and Variable-Speed Drives*.

[8] Liu, Jianqiang, Lin, Fei, Yang, Zhongping, and Zheng, Trillion Q. “Field oriented control of linear induction motor considering attraction force & end-effects”. In: *2006 CES/IEEE 5th International Power Electronics and Motion Control Conference*. Vol. 1. IEEE. 2006, pp. 1–5.

[9] Mohamed, Essam EM, Sayed, Mahmoud A, and Mohamed, Tarek Hassan. “Sliding mode control of linear induction motors using space vector controlled inverter”. In: *2013 International Conference on Renewable Energy Research and Applications (ICRERA)*. IEEE. 2013, pp. 650–655.

[10] Musk, E. “Hyperloop White Paper”. In: *dated Aug* 12 (2013).

[11] NJ, Merlin Mary, Ganguly, Chandrajit, and Kowsalya, M. “Simulation of Linear induction Motor using Model Predictive Control in synchronously rotating reference frame”. In: *2016 IEEE 1st International Conference on Power Electronics, Intelligent Control and Energy Systems (ICPEICES)*. IEEE. 2016, pp. 1–5.

[12] Nounou, Hazem N and Rehman, Habib-ur. “Application of adaptive fuzzy control to ac machines”. In: *Applied soft computing* 7.3 (2007), pp. 899–907.

[13] Roncero-Sánchez, Pedro, García-Cerrada, Aurelio, and Feliu-Batlle, Vicente. “Rotor-resistance estimation for induction machines with indirect-field orientation”. In: *Control Engineering Practice* 15.9 (2007), pp. 1119–1133.

[14] Sun, Xiao, Shi, Liming, Zhang, Zhihua, and Zhu, Haibin. “Thrust control of a double-sided linear induction motor with segmented power supply”. In: *IEEE Transactions on Industrial Electronics* 66.6 (2018), pp. 4891–4900.

[15] Sung, Jeong-hyoun and Nam, Kwanghee. “A new approach to vector control for a linear induction motor considering end effects”. In: *Conference Record of the 1999 IEEE Industry Applications Conference. Thirty-Forth IAS Annual Meeting (Cat. No. 99CH36370)*. Vol. 4. IEEE. 1999, pp. 2284–2289.

[16] Team, KTH Hyperloop. *KTH Hyperloop Final Report*. 2019.

[17] Team, MIT Hyperloop. *MIT Hyperloop Final Report*. 2017.

[18] Vaez-Zadeh, S and Satvati, MR. “Vector control of linear induction motors with end effect compensation”. In: *2005 International Conference on Electrical Machines and Systems*. Vol. 1. IEEE. 2005, pp. 635–638.

[19] Vasudevan, M, Arumugam, R, and Paramasivam, S. “Development of torque and flux ripple minimization algorithm for direct torque control of induction motor drive”. In: *Electrical Engineering* 89.1 (2006), pp. 41–51.

[20] Yamamura, Sakae. “Theory of linear induction motors”. In: *New York, Halsted Press, 1979. 246 p.* (1979).

[21] Yu, Jianfeng, Zhang, Ting, and Qian, Jianming. *Electrical Motor Products: International Energy-Efficiency Standards and Testing Methods*. Elsevier, 2011.

Appendix - Contents

Appendix A

First Appendix

The matlab code used for the simulation is shown below:

```
clear all
%s subscript means stator/primary
%r subscript means rotor/secondary/linor
%Parameters from MPC paper referred as number 11

Rs = 1.298;   %Primary resistance
Rr = 0.976;   %Secondary resistance
R_s=Rs;
R_R=Rr;
Ls=0.0684;    %Primary inductance
Lr=0.0416;    %Secondary inudctance
Lm =0.0416;   %magnetization inductance; %magnetization inductance
L_M=Lm;
L_ls = Ls-Lm;       %stator/primary leakage inductance
L_lr = Lr-Lm;       %rotor/secondary leakage inductance
Ll=L_ls+L_lr;
L_alpha=Ls*Lr-Lm^2;
tau=0.14;           %obtained from paper
%pole pitch in meters   %w=pi/tau*v or w=pi/(2*tau)*v
p = 4; %pole pairs
%D = 0.1; %Viscous damping
m = 10;             %Mass of motor
L=1;                %length of LIM

L_sigma=L_ls+L_lr;  %Sum of leakage inudctance
```

```
R_R_hat=Rr;
%all the hat terms are estimated value, currently taken as actual value
R_hat=Rs+Rr;
L_M_hat=Lm;          %Magnetizing inductance
L_sigma_hat=L_sigma;

psi_ref=1*250/(100*pi); %steady state value
%psi_ref=1*450*sqrt(2/3)/100/pi;
id_ref=psi_ref/L_M_hat;   %id controls the flux
iq_ref=0.5;
%Only when we do not use speed controller and iq control the torque

m_hat=m;

%Current controller
tr=1e-3;
alpha_c= (log(9)/tr);
Ra= alpha_c*L_sigma_hat-R_hat; %active resistance used for minimising
%steady state error
kp_c=alpha_c*L_sigma_hat; %chapter 4
ki_c=alpha_c*(R_hat+Ra);
%ki_c=alpha_c*R_hat;
V_sat=415*sqrt(2/3);


%Speed Controller
alpha_s=1/120*alpha_c;
K=2/3;
%ba=(alpha_s*J_hat-b_hat)/psi_ref;
kp_s=alpha_s*m_hat/psi_ref;
ki_s=alpha_s^2*m_hat/psi_ref;
iq_max=sqrt(100^2-id_ref^2); %This value has to be figured out according to motor curren


%Field weakening chapter 9
I_nom=psi_ref/L_M_hat;
I_min=0.1*I_nom;
Vbase=250;
zeta=(L_sigma_hat+L_M_hat)/L_sigma_hat;
```

```
%iq_ref_nom=1;
I_max=3*I_nom;    %Value of I_max
wbase_fw=50*2*pi;
```